Expression and function of the transcription factor *Rx* in *Nematostella vectensis*

By

Benjamin Lerstad

This thesis is submitted in partial fulfilment of the requirements for the degree of

Master of Science

Department of Biological Sciences

Faculty of Mathematics and Natural Sciences

University of Bergen

June 2023

Acknowledgments

The work presented in this thesis was conducted in the Rentzsch group at the Department of Biological Science, University of Bergen.

It has been an amazing experience to be a part of the Rentzsch lab environment, largely due to the people I have gotten to work alongside. Most of all, I would like to thank my supervisor **Fabian Rentzsch**, and my co-supervisor **Natascha Bartsch**. **Fabian**, thank you for giving me the opportunity to work on this interesting project, and for always finding time for me when I had questions. I appreciate all the feedback you have provided, and for boosting my confidence when I needed it. **Natascha**, thank you for teaching me everything in the lab. Thank you for being so kind and patient, and for always trying to answer my many questions. You have taught me so much, and I could not have done this without your help. **Alexis**, thank you for being the big sister of the lab, always providing help whenever I asked, but also for being strict when it was needed. **Fatemeh**, thank you for our nice conversations and for calming me down whenever I was stressed. I would also like to thank **Eilen** for taking care of all the animals.

Thank you to all my fellow master students, especially **Sarah** and **Maria**, for your friendship and our great laughs while in the lab. I would also like to thank my roommates, **Live** and **Benjamin**, for creating such a comfortable atmosphere in the apartment. **Umar** and **Rune**, my best friends, thank you brightening up my days.

Finally, I would like to thank my family for all the support they have shown me during my studies. Thank you for always making time to talk over the phone, and for trying to give me advice even when you barely understand what I am doing. I would have never gotten this far without your love and support.

Thank you, tusen takk!

Benjamin Lerstad   Bergen, June 2023

Table of Contents

Selected abbreviations

Ash - Achaete scute

Ath - Atonal

CNS - Central nervous system

FISH - Fluorescence *in-situ* hybridization

Fox - Forkhead box

GFP - Green fluorescent protein

ISH - *In-situ* hybridization

NCC - Neural crest cell

NPC - Neural progenitor cell

NSC - Neural stem cell

Nv - *Nematostella vectensis*

PNS - Peripheral nervous system

Pax – Paired box

RGC - Radial gland cell

RT - Room temperature

Rx - Retinal homeobox

Sox - SRY-box transcription factors

TF - Transcription factor

WT - Wild type

bHLH - Basic helix-loop-helix

cDNA - Complimentary DNA

dpf - Days post fertilization

gDNA - Genomic DNA

hpf - Hour's post fertilization

sgRNA - Single guide RNA

sh*GFP* - GFP shRNA

sh*NvRx* - *NvRx* shRNA

shRNA - Short hairpin RNA

Abstract

The development of the central nervous system is highly studied and a comparatively well understood field of neurogenesis. The fundamental aspects of neurogenesis have however mostly been studied in a select few bilaterian model organisms, leaving many questions regarding the evolution of this process open. The cnidarian and bilaterian lineages are sister groups that separated approximately 600 million years ago. Cnidarians occupy an informative phylogenetic position to study the early evolution of cellular and molecular aspects of neurogenesis, and to understand common principles of neural development. The Cnidaria sea anemone *Nematostella vectensis* has in recent years emerged as one of the most tractable cnidarian models for the study of neurogenesis and development in an evolutionary context. The later steps of neural differentiation in *Nematostella* are yet to be fully understood. Neuronal markers have been found for different neural sub-populations, one of which is the transcription factor *NvFoxQ2d* that gives rise to sensory cells in *Nematostella*. Although the function of *NvFoxQ2d* is yet to be determined, studies are being performed to further understand this transcription factor, one of which is a transcriptome of the fluorescent cells in the *NvFoxQ2d*::*mOrange* transgenic reporter line. During the analysis of this dataset, the transcription factor *NvRx* was found to be highly upregulated in this cell population. While the Retinal homeobox gene (*Rx*) has a well-described role in the formation of the retina, and the formation and proliferation of retinal progenitor cells in vertebrates, the function of *NvRx* in the eyeless *Nematostella* is in contrast yet to be determined.

By performing a double fluorescence *in-situ* hybridization, we show that *NvRx* is expressed in the majority of the *NvFoxQ2d* cell population. We hypothesised that *NvRx* could play a role in the regulation of these *NvFoxQ2d*-expressing cells, and by performing an *in-situ* on embryos injected with *NvRx* shRNA injection, we show that *NvRx* acts as an upstream regulator of *NvFoxQ2d*. We also found *NvRx*-expressing cells in close proximity to *NvElav1*-expressing neural cells, indicating that these cells could be descended from the same progenitor cells. Finally, a CRISPR/Cas9 mediated mutant line was successfully generated to further study the function of *NvRx* in *Nematostella* development.

1 Introduction

1.1 Neurogenesis

As animals evolved from unicellular organisms, more complex structures were able to develop by specializing cells within the organism. With the evolution of contraction-based motility, a mechanism to coordinate these cells was evolved in parallel. These specialized cells, so-called proto-neurons, are thought to be evolved from chemo- or mechanosensory epithelial cells that could respond to stimuli, initiating a response in neighbouring cells. As the organisms became bigger, these cells diversified further into what we define as neurons today (Kristan, 2016). Neurons are a diverse group of highly polarized cells, meaning that they have an asymmetric morphology, typically consisting of the soma (cell body with the nucleus), dendrites, axons, and axon terminals (Lodish et al., 2016, pp. 1026–1029). Neurons can transmit signals to other neurons through neurotransmitters released at the synapse, a connection between dendrites and axon terminals. When a signal enters the dendrites through neurotransmitter receptors, an electrical charge is generated within the dendrite which is then transmitted to- and interpreted in the soma and passed to the axon hillock, the connection between the axon and the soma. If the electrical signal is strong enough to pass the threshold potential, roughly -55mV, the signal is passed to the axon. In the axon, voltage gated sodium channels open and cause a depolarization of the cell. The depolarization cascade along the membrane causes a rapid change of voltage across the membrane called an action potential. This action potential travels down the axon until it reaches the axon terminals, where neurotransmitters are released (Lodish et al., 2016, pp. 1026–1029). Neurons can broadly be classified into three groups based on their interaction. Sensory neurons respond to stimuli and send this information to the central nervous system, where it can be interpreted either in the spinal cord or the brain. Motor neurons transmits signals from the central nervous system to muscle- or gland cells. Interneurons connects neurons to other neurons, allowing communication between sensory neurons, motor neurons and the central nervous system (Campbell et al., 2018, p. 1125).

1.2 Development of the vertebrate nervous system

The development of the central nervous system (CNS) in vertebrates is a highly studied and a comparatively well understood field of neurogenesis. The CNS can be divided into two main sections, the brain, and the spinal cord. The spinal cord mainly functions as a highway connecting the brain and the peripheral nervous system (PNS), allowing signals from the PNS to be processed by the brain, and allowing signals from the brain to reach different parts of the body. The formation of the CNS is a precisely regulated process needing timely cues from patterning signals to activate or deactivate transcription factors at the transcriptional or posttranscriptional level (Hartenstein & Stollewerk,

2015). With the establishment of an anterior-posterior and dorsal-ventral axis during gastrulation, neural stem cells (NSC) arise in an area on the dorsal ectoderm called the neuroectoderm. The neuroectoderm can be divided into two structures, the neural plate which will form the neural tube, and the neural plate border containing the neural crest cells (NCC). During neurulation, the neural plate invaginates forming the neural groove. The neural plate border folds over the neural groove and fuses, closing the neural groove and forming the neural tube. The neural crest cells delaminate from the non-neural ectoderm and the neural tube, which then separates the neural tube from the ectodermal layer (Campbell et al., 2018, pp. 1084–1085). The neural tube will form the CNS, while the PNS is formed by the NCC. The anterior-most region of the neural tube will form the forebrain, followed posteriorly with the midbrain and hindbrain. The most posterior region of the neural tube will form the spinal cord (Hartenstein & Stollewerk, 2015). After the formation of the neural tube, at the onset of neurogenesis, the neuroectodermal cells switch their identity and turn into radial glial cells (RGC), which are directly or indirectly responsible for the formation of all neurons and glial cells during neurogenesis. These RGCs then switch from symmetric self-renewing divisions to asymmetric divisions, giving rise to a RGC daughter cell and a differentiating cell. These differentiating cells can either turn into a neuron, or in some parts of the brain, turn into an intermediate progenitor which, via symmetric division, turns into two neurons (Paridaen & Huttner, 2014). In the last step of neurogenesis, the newly formed neurons migrate to their final destination where they mature, forming dendrites and axons, and become part of the neuronal circuits (Rahimi-Balaei et al., 2018). While neurogenesis and its transcriptional regulation has been studied in detail in a few model organisms, it remains poorly understood how this complex process may have looked like in early evolved animals.

1.3 Cnidaria

Cnidarians separated from the lineage that led to the emergence of bilaterians more than 600 million years ago. As an outgroup to Bilateria, they occupy an informative phylogenetic position for understanding the evolution of the nervous system (**Figure 1**) (Rentzsch et al., 2017). By comparing the similarities and differences in the development of neural structures in Cnidaria and Bilateria, it can give key insights into the evolution of the nervous system.

Cnidaria consist of two major clades, the anthozoans and the medusozoans, which separated not long after the cnidarian lineage separated from all other animals (Rentzsch et al., 2017). The Anthozoa consist of Hexacorallia and Octocorallia, and the Medusozoa consist of Hydrozoa, Scyphozoa, Cubozoa, Myxozoa and Staurozoa. Hexacorallia are categorized by a 6-fold symmetry and includes sea anemones, while Octocorallia are categorized by an 8-fold symmetry. Two distinct body plans can be

observed in cnidarians: the sessile polyps, a tubular body with a single body opening surrounded by prey-catching tentacles; and medusae, an umbrella-shaped bell with trailing tentacles (Rentzsch et al., 2017). While both Anthozoa and Medusozoa have sessile polyps, the distinguishing feature between the clades is the gamete-producing free-swimming medusae stage of the Medusozoan life cycle (Rentzsch et al., 2017; Technau & Steele, 2011).

One key difference in body plan between the triploblastic bilaterians and the diploblastic cnidarians is the number of germ layers. Bilateria have the three germ layers endoderm, mesoderm and ectoderm, while Cnidaria only have two germ layers, ectoderm and mesendoderm (Martindale et al., 2004). The cnidarian mesendoderm has properties associated with both meso- and endoderm, possessing cells associated with digestion and nutrient uptake which resembles the bilaterian endoderm, and various myoepithelial cells responsible for body contractions which resembles bilaterian mesoderm (Layden et al., 2016; Steinmetz et al., 2017). The cnidarian germ layers are separated by the mesoglea. The mesoglea consists of an extracellular matrix as well as some neurites extending from ectodermal and mesendodermal neurons (Layden et al., 2016). While neurons in Bilateria originate from the ectodermal tissue, both the ectoderm and mesendoderm layers produce neurons and nerve nets in Cnidaria (Kelava et al., 2015). The cnidarian nervous system is made up of three classes of cells, sensory cells, ganglion cells and the Cnidaria-specific cnidocytes (Rentzsch et al., 2017).

As genetic tools became available for different species, the anthozoan sea anemone *Nematostella vectensis* emerged as one of the most tractable cnidarian models for developmental research (Layden et al., 2016).
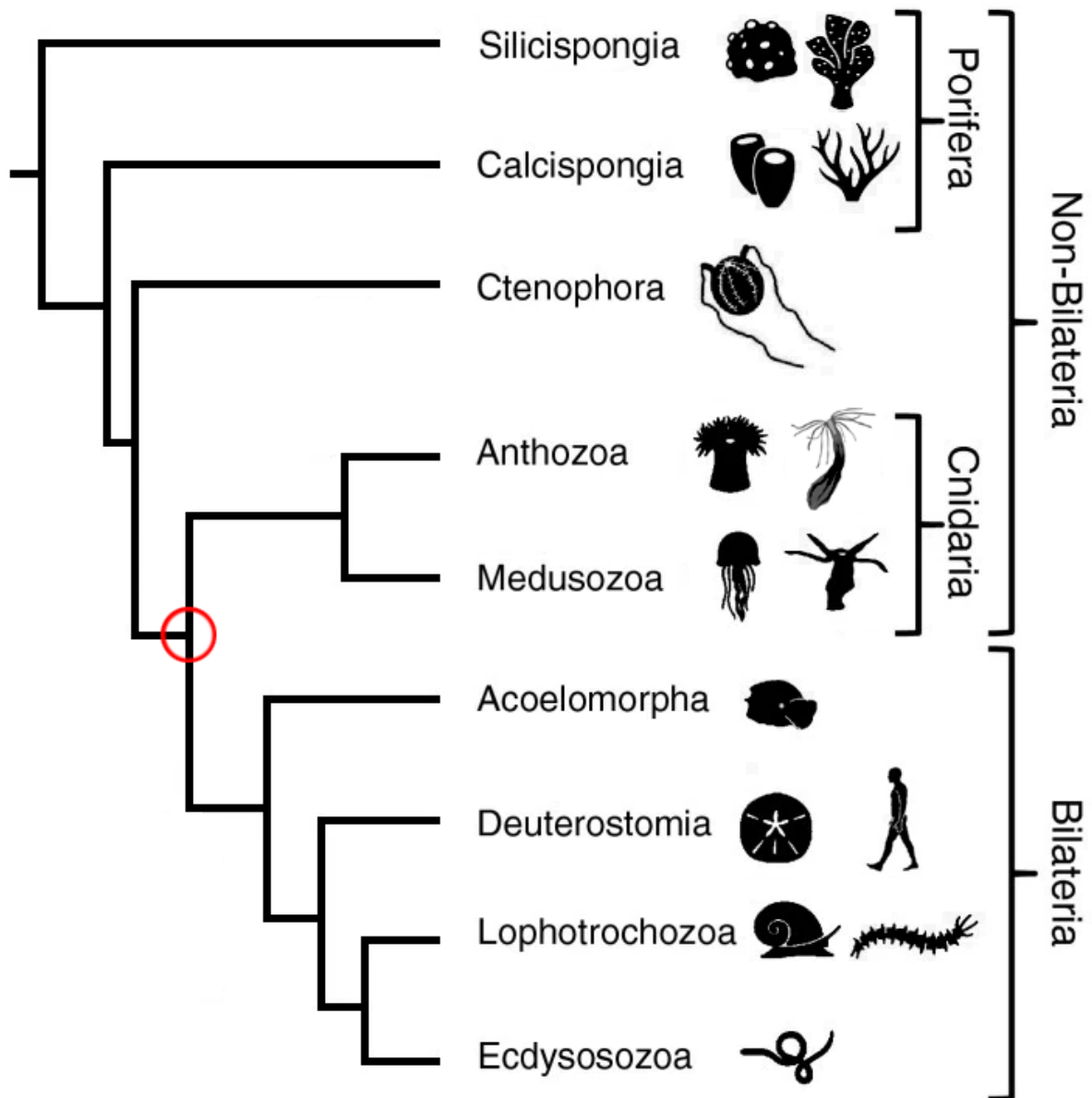
Figure 1: Phylogenetic relationship of the major metazoan clades. The phylogenetic tree shows that Cnidaria are the sister taxon of Bilateria. The red circle indicates the position of the last common ancestor of cnidarians and bilaterians. Figure modified from (Ryan et al., 2006)

1.4 *Nematostella vectensis* as a model organism

Nematostella vectensis, commonly known as the Starlet Sea anemone, is a sea anemone species native to the Gulf of Mexico and the straits of Florida, with established non-native populations observed on the west coast of United states and in the Irish- and North Sea. *Nematostella vectensis* is a small estuarine, euryhaline burrowing sea anemone, and has been recorded in salinities of 0.9 to 5.1% (Hand & Uhlinger, 1992). The natural habitat of *Nematostella vectensis* is mud or silt planes within brackish waters, where it burrows its body column, leaving only the oral opening and tentacles protruding from the sediment. The body column of *Nematostella vectensis* can reach a length of 1-2 cm in its natural

habitat, but when kept in culture it can reach a length of 10cm (Hand & Uhlinger, 1992). *Nematostella vectensis* has gained popularity as a model system over the last two decades following a 1992 publication laying out a protocol for culturing and spawning the animal throughout its life cycle (Hand & Uhlinger, 1992).

Nematostella vectensis has two main body axes. The primary oral–aboral axis, which runs from the oral opening to the opposite aboral side, and the secondary axis (directive axis), which is oriented orthogonal to the oral–aboral axis. The mesendoderm has 8 radially repeated infoldings called the mesenteries that run along the oral-aboral axis (**Figure 2A-C**). The mesenteries contain the somatic gonads, nutrient storage, digestive tissue, cnidocytes (stinging cells) and retractor muscles (**Figure 2D**). Towards the oral pole, the mesenteries connect with the pharynx (**Figure 2B**), and the oral opening surrounded by up to 16 tentacles (Layden et al., 2016; Steinmetz et al., 2017).
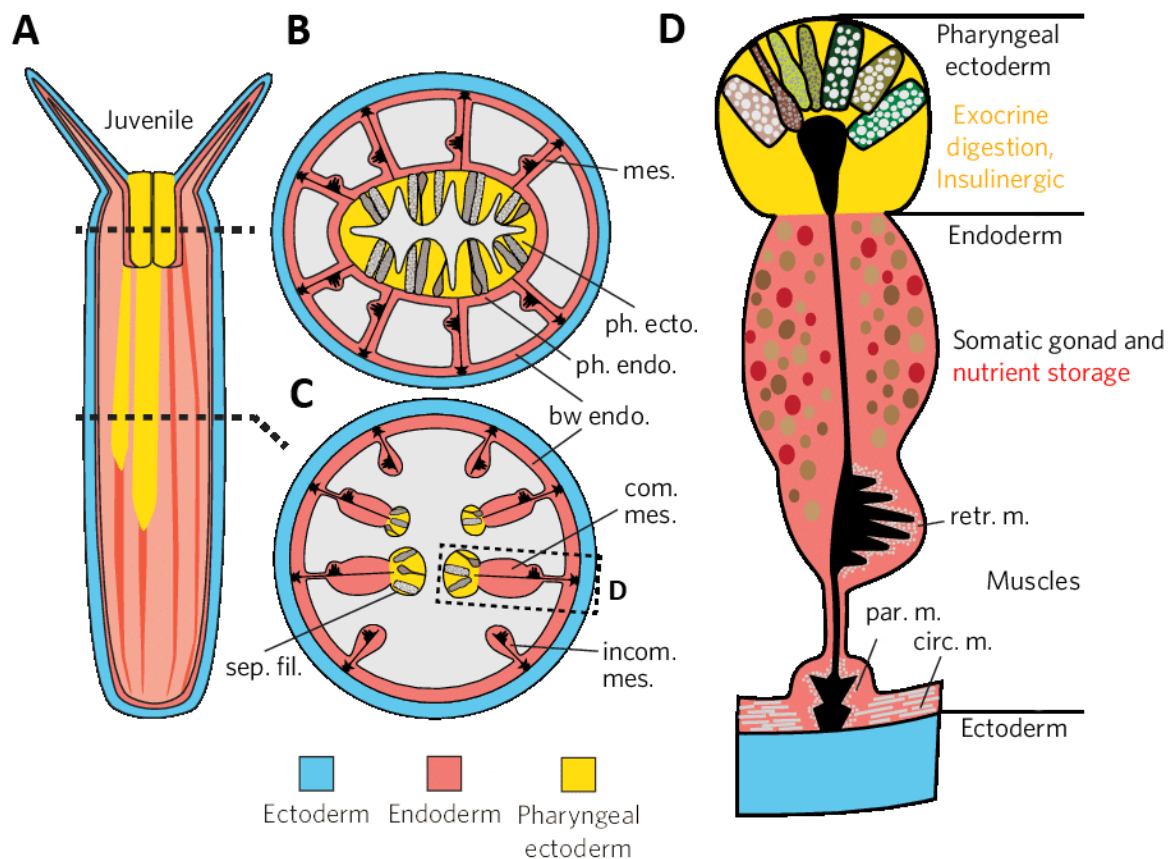
Figure 2: Morphological schematic of a juvenile *Nematostella vectensis*. (A) The body column of a juvenile animal showing the different germ layers. **(B)** Cross-section of the pharynx region showing the pharyngeal ectoderm (Yellow), pharyngeal endoderm (Red) and ectoderm (Blue). The directive axis can be observed horizontally. **(C)** Cross-section of the body column showing the distribution of the complete and incomplete mesenteries that spans the oral-aboral axis of the body column. **(D)** Close-up of a complete mesentery showing the different muscles, somatic gonads and nutrient storage located in the mesendoderm (here called endoderm), and the pharyngeal ectoderm tissue containing the exocrine and insulinergic cells responsible for extracellular digestion. bw (body wall); circ. m. (circular muscle); com. mes. (complete mesentery); ecto. (ectoderm); endo. (endoderm); incom. mes. (incomplete mesentery); par. m. (parietal muscle); ph. (pharynx); retr. m. (retractor muscle); sep. fil. (septal filament). Figure modified from (Steinmetz et al., 2017).

1.4.1 Life cycle of *Nematostella*

Although *Nematostella vectensis* normally reproduce via dioecious reproduction, where individuals produce only one type of germ cells, they are also able to reproduce asexually via two specific types of budding, polarity reversal and physal pinching (Röttinger, 2021). The growth and development of the animals is temperature-dependent, and the entire life cycle can be completed in 8-12 weeks with optimal conditions (Layden et al., 2016; Röttinger, 2021). Because the developmental lifecycle is temperature-dependent, timepoints are defined as hours post fertilization (hpf) at 21°C.

During sexual reproduction (**Figure 3**), the gametes are produced in the mesenteries. During oogenesis, the eggs are squeezed through the epithelium of the mesenteries into the gastric cavity, then embedded in a gelatinous mucoid mass before being released through the oral opening (Hand & Uhlinger, 1992). Unfertilized eggs have a clear animal-vegetal polarity. The animal pole of the egg is defined by the location of the female pronucleus, which is located close to the cell membrane (Fritzenwanker & Technau, 2002). The egg packages, containing up to 200 eggs, are then fertilized externally by free-swimming sperm released by the male (Hand & Uhlinger, 1992). In culture, gametogenesis is induced by a light and temperature shift (Fritzenwanker & Technau, 2002). Once fertilized, the zygote undergoes a series of cleavages where the first two divisions originate at the animal pole (Lee et al., 2007). Early cleavages in *Nematostella* are characterized as asynchronous chaotic cleavage, where at times, odd number of cells undergo cleavage (Reitzel et al., 2007). The cleavage stages give rise to a ciliated coeloblastula at approximately 8hpf, and the oral-aboral polarity can be observed morphologically during gastrulation at approximately 20hpf (Lee et al., 2007). During gastrulation, the pre-mesendodermal plate, indicated in orange in **Figure 3**, invaginates into the blastocoel and adheres to the basal side of the ectoderm. The forming gastrula will also internalize ectoderm which becomes the pharynx and distal part of the mesenteries (the septal filaments) (Steinmetz et al., 2017; Technau, 2020). In the planula stage, approximately 36hpf, the animal elongates along the oral-aboral axis and emerges from the egg jelly (Lee et al., 2007). In the later stages of the planula stage, approximately 48hpf, the animal generates an apical tuft on its aboral pole. A couple of days after emerging from the jelly, the free-swimming planula develops four primary tentacle buds surrounding the oral pole. By day seven, the animal develops into a four-tentacle primary polyp, loses its apical tuft and settles to the substrate and begins feeding (Lee et al., 2007). The animal then grows with access to nutrients, reaching sexual maturity at approximately 8-12 weeks post fertilization (Layden et al., 2016; Röttinger, 2021).
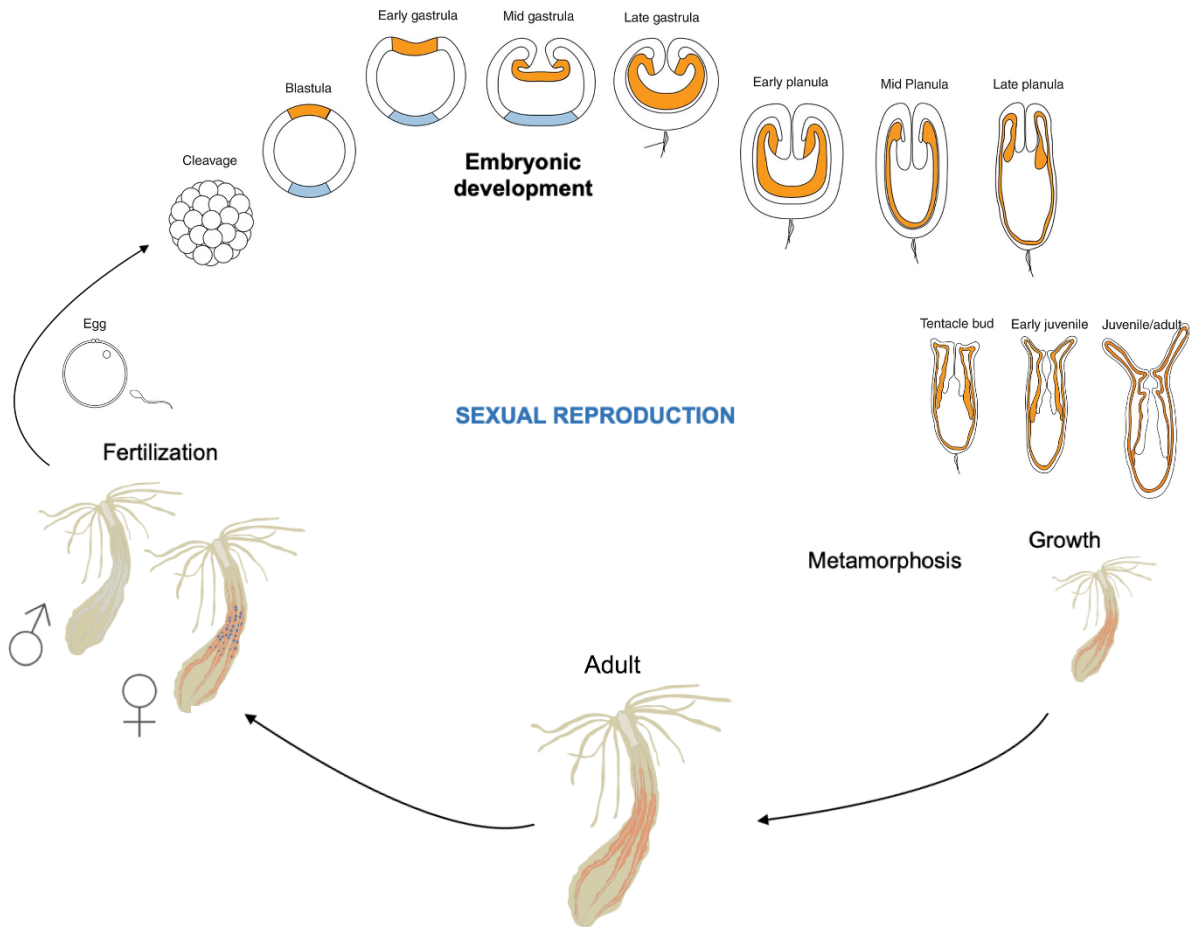
Figure 3: Schematic displaying the life cycle and development of *Nematostella vectensis*. (A) Sexual reproduction: Adult Nematostella releases gametes that are fertilized externally. The fertilized egg goes through cleavage (1-8hpf), blastula stage (8-20hpf), gastrula stage (20-36hpf), planula stage (36-96 hpf), primary polyp (3-7dpf) then juvenile to adult. Orange indicates the pre-mesendodermal plate in blastula and gastrula, and the mesendoderm in planula and juvenile. Blue indicates the future apical tuft region. Figure modified from (Layden et al., 2016; Röttinger, 2021)

1.4.2 Neurogenesis in *Nematostella*

In contrast to most bilaterians where nerve cells are exclusively generated within the ectoderm, both the ectodermal and mesendodermal layer generate neurons in *Nematostella vectensis*. The nervous system in *Nematostella* is described as a nerve net with two interconnected neuronal networks, one in the ectodermal layer and one in the mesendodermal layer (Kelava et al., 2015). The nervous system consists of three main classes of neural cells; sensory cells, ganglion cells, and the cnidarian specific cnidocytes, with each class compromising of several subpopulations expressing for example different neuropeptides (Kelava et al., 2015). Sensory neurons and ganglion neurons are found in both the ectoderm and mesendoderm, whereas cnidocytes are exclusively found in the ectoderm. Neural progenitor cells (NPC) are first observed during the blastula stage (**Figure 4A,** blastula). During the early gastrula stage, some of these NPCs differentiate, giving rise to the ectodermal nervous system. As the invagination is finishing during late gastrula, NPCs start to appear in the mesendodermal layer

13

(**Figure 4A**, early planula). During the planula stages, the mesendodermal NPCs give rise to the mesendodermal nervous system (**Figure 4A**, late planula) (Richards & Rentzsch, 2014). As the neural cells are developing, they project neurites throughout the tissue, connecting to other neurons, forming the nerve net that can be observed in the polyp stage (**Figure 4A**, primary polyp) (Nakanishi et al., 2012).
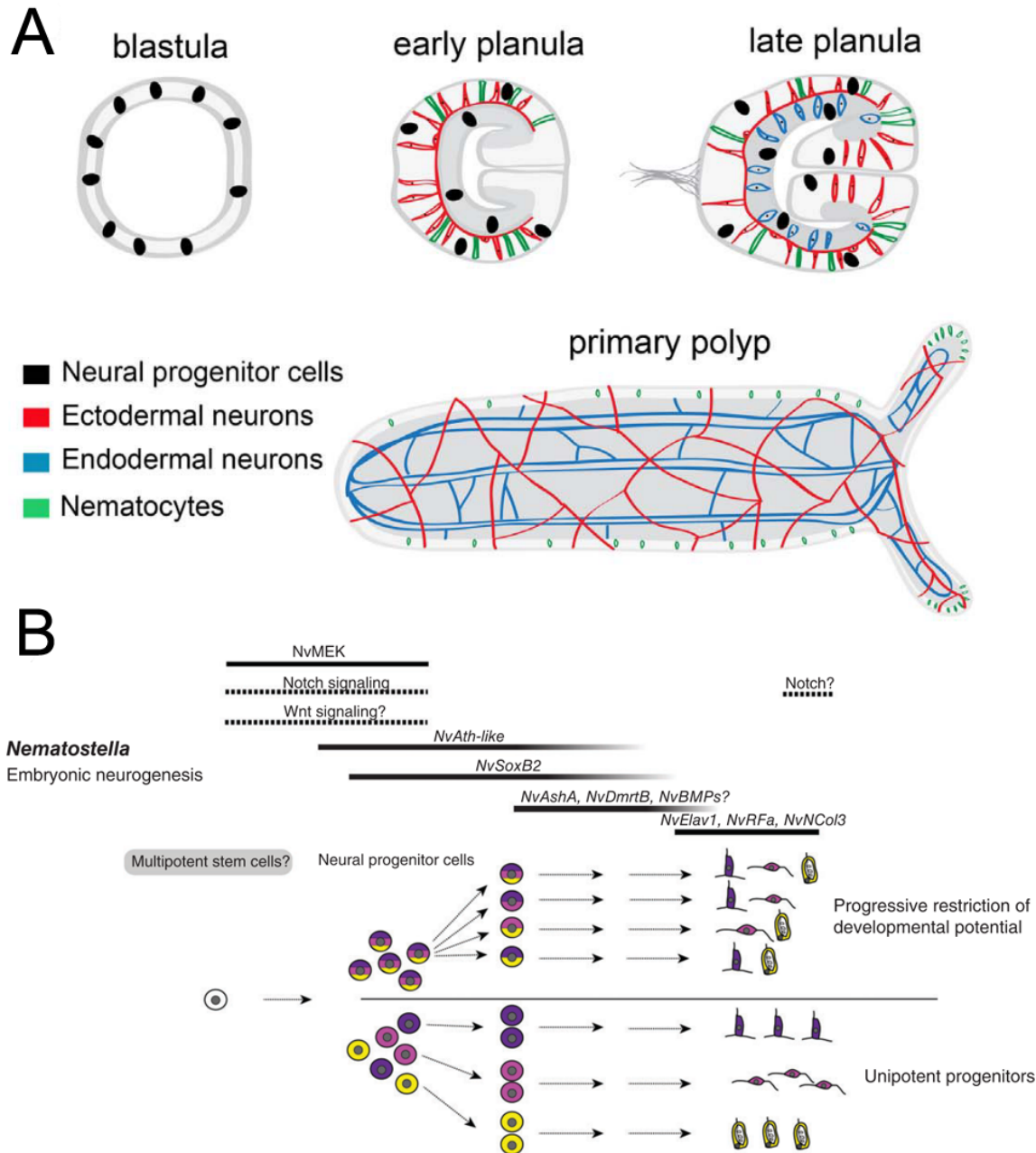
Figure 4: Schematic representation of the development of the nervous system in *Nematostella*. (A) Overview of nervous system development in *Nematostella*. Neural progenitor cells are detectable at the blastula stage. Differentiating neurons are present in the ectoderm from gastrula stage onwards, while neurons the mesendoderm is first seen at planula stage. The nervous system of the primary polyp is mainly organized as nerves net with prominent tracts of mesendodermal neurites running along the mesenteries. **(B)** A pool of dedicated neural progenitor cells gives rise to the tree major classes of neural cells (sensory cells, ganglion cells, and nematocytes) during embryogenesis. These cells may give rise to different classes of neurons through asymmetric divisions (upper part), or to only one class of neural cells through symmetric

Studies have shown a remarkable level of similarity between *Nematostella* and bilaterian neurogenesis. One of the earliest expressed genes in the neural ectoderm of vertebrates are the sox family of transcription factors (TF) which is required for neurogenesis. Expression of sox genes has been characterized in *Nematostella*, and *NvSoxB2* (also referred to as *NvSoxB(2)* and *NvSoxB2a* in literature), one of five genes closely related to the bilaterian SoxB TF family, has been shown to be expressed in proliferating cells (Magie et al., 2005). To study the progeny of the *NvSoxB2*-expressing cells, a transgenic reporter line was generated where the *NvSoxB2* promoter drives the expression of mOrange (a fluorescent protein) (Richards & Rentzsch, 2014). The mOrange signal can persist for a period of time even after expression of the gene of interest has stopped, and by observing the fluorescent progeny in this reporter line, it was shown that the *NvSoxB2*-expressing population has the developmental potential to give rise to sensory neurons, ganglion neurons, secretory cells and cnidocytes (Layden et al., 2016; Rentzsch et al., 2020; Richards & Rentzsch, 2014; Tournière et al., 2022). Morpholino mediated knockdown experiments have also shown that when *NvSoxB2* is not expressed, the population of neurons is strongly reduced (Kelava et al., 2015). These observations indicate that *NvSoxB2* plays a crucial part in the regulation of NPC development (Richards & Rentzsch, 2014). With *NvSoxB2* expression being observed in the initial neural progenitor population, it has become the marker for NPCs in *Nematostella*. Cellular markers are proteins specific to a certain population of cells (Redwine & Evans, 2002).

Another family of transcription factors that has been found to play a role in early neurogenesis in *Nematostella* is the basic helix-loop-helix (bHLH) family of TFs (Rentzsch et al., 2017). "Proneural genes" are genes which move cells out of their progenitor state, triggering neural differentiation (Hartenstein & Stollewerk, 2015). bHLH proneural genes belonging to the achaete-scute and atonal families are highly conserved in bilaterian neurogenesis (Rentzsch et al., 2017). An achaete-scute homologue (*ash*) gene, *NvAshA*, has been found to promote neurogenesis in *Nematostella* by regulating both the ectodermal and mesendodermal neural development during early neurogenesis (Layden et al., 2012). Knockdown studies of *NvAshA* have shown that several neuronal markers, including *NvAnthoRFamide* and *NvElav1,* have reduced expression in the absence of *NvAshA* expression (Layden et al., 2012). Unlike in bilaterians where *ash* genes are expressed in both proliferative progenitor/stem cells and early differentiating neurons, *NvAshA* appears restricted to non-dividing cells where they co-express with *NvSoxB2* (Rentzsch et al., 2017; Richards & Rentzsch, 2015). Another bHLH proneural gene, *NvAth-like,* is however co-expressed with *NvSoxB2* in dividing

NPCs. The loss of *NvAth-like* function results in a decrease in the expression of *NvAsh* and *NvSoxB2,* as well as other neural markers such as *NvElav1 and NvNcol3* (Richards & Rentzsch, 2015). This suggests that *NvAth-like* and *NvSoxB2* promote neurogenesis and are involved in the specification of NPCs, while *NvAshA* is involved in neural differentiation during later stages of neurogenesis (**Figure 4B**) (Richards & Rentzsch, 2015).

The Notch signalling pathway plays an essential role in the regulation of both embryonic and adult neurogenesis in vertebrates. Delta-Notch signalling regulates neurogenesis through the process of lateral inhibition where the Notch ligands Delta or Jagged activate Notch receptors on directly adjacent cells. The received signal then leads to the release and nuclear localization of the Notch intracellular domain (NICD), where it functions as a transcription factor, mediating the transcription of Hes genes which in turn repress the expression of bHLH proneural genes (Paridaen & Huttner, 2014). Through functional studies in *Nematostella*, where Notch signalling is inhibited by the γ-secretase inhibitor DAPT, the Notch signalling pathway has been shown to regulate and suppress neural development by suppressing the expression of the *NvSoxB2* and *NvAth-like* transcription factors (Kelava et al., 2015).

The later steps of neural differentiation in *Nematostella* are yet to be fully understood. Neuronal markers have been found for different neural sub-populations, and by creating transgenic lines for these populations, one can study these in more detail. One example of a transgenic line which is used to study a sub-population of neurons is the *NvFoxQ2d*::*mOrange* transgenic line. The transcription factor *NvFoxQ2d* has been identified in unipotent progenitor cells deriving from *NvSoxB2*-expressing NPCs, giving rise to putative sensory cells in *Nematostella* (Busengdal & Rentzsch, 2017). Although the function of *NvFoxQ2d* is yet to be determined, studies are being performed to further understand this transcription factor, one of which is a transcriptome of the fluorescent cells in the *NvFoxQ2d*::*mOrange* transgenic line (Gahan, Kouzel, Bartsch and Rentzsch, unpublished data). Analysis of this dataset has revealed several highly upregulated transcription factors, one of them being *NvRx*. The expression pattern of *NvRx* has been characterized in *Nematostella* by Mazza et al., where they found expression in the aboral side of the ectodermal layer from mid-gastrula stage through the planula stages (**Figure 5C-J**). Expression of *NvRx* was also found in the ectoderm of the tentacles in the primary polyp (**Figure 5K**) (Mazza et al., 2010).
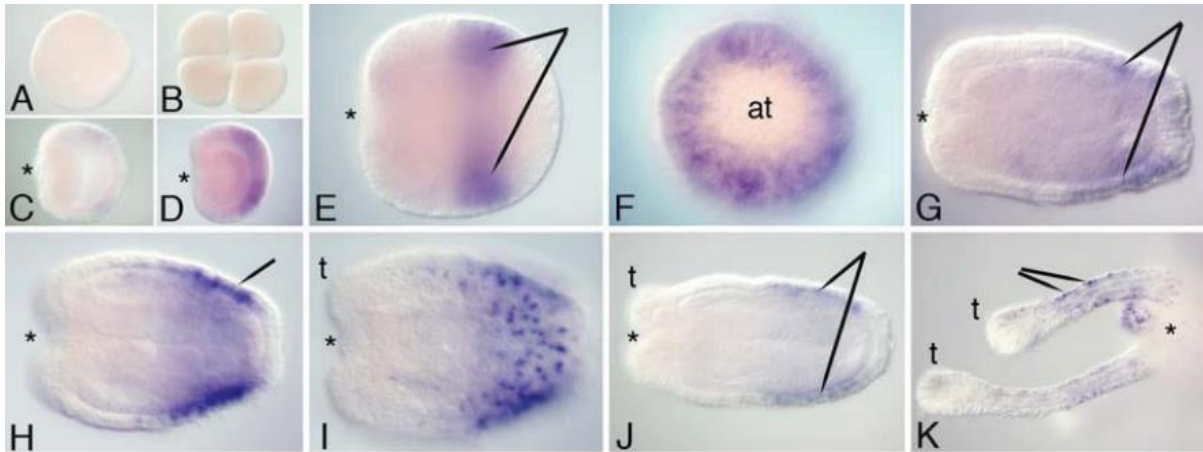
Figure 5: Expression of *NvRx*. *In-situ* hybridization of *NvRx* in wild type animals. **(A-B)** No expression is detected in the egg or in the early cleavage stages. **(C-D)** Expression is observed around the aboral ectoderm during early to mid-gastrula stages. **(E)** Late gastrula stage showing a uniform band of expression in the aboral ectoderm. **(F)** The same embryo in (E) viewed from the aboral pole, showing a lack of expression in the future apical tuft region. **(G-J)** Planula stages shows expression as scattered cells on the aboral side of the animal, with (I) showing the surface view. **(K)** Close-up of the tentacles in the polyp stage shows expression in the ectoderm of the tentacles. (at) denotes future apical tuft region, (t) denotes tentacle buds and tentacles, asterisks denote the oral opening. Figure adapted from (Mazza et al., 2010).

1.5 Retinal homeobox

Retinal homeobox (*Rx*), also known as Retinal and anterior fold homeobox, is a paired-like homeodomain transcription factor consisting of an octapeptide motif on the N-terminus, a highly conserved homeodomain, and an OAR domain on the C-terminus. A nuclear localization signal can also be found on the C-terminus. The homeodomain consists of a bHLH motif which binds the protein to the DNA strand. The function of the octapeptide motif and the OAR domain has not yet been established, however, these motifs are usually also found in other paired-type homeobox proteins (Furukawa et al., 1997).

The retinal homeobox gene was first identified in 1997 by Furukawa et al., while they were trying to identify genes involved in the development of the vertebrate eye (Furukawa et al., 1997). By using *in-situ* hybridization on mouse embryos, they found an initial expression of *MRx* (Murine *Rx*) in parts of the anterior neural fold which gives rise to the ventral forebrain and optic vesicles. Later in the developing embryo, the gene is restricted to the optic vesicles and ventral diencephalon, with expression eventually stopping in the ventral diencephalon. As the retina develops within the optical structure, *MRx* can be found in the zone of proliferating cells, and after birth, the expression gradually decreases as proliferation declines (Furukawa et al., 1997).

To further understand the regulation of vertebrate eye development by *Rx*, Bailey et al., performed knockout studies on mice where they eliminated the *Rx* gene, and knockdown studies on Xenopus using *Rx* morpholinos (Bailey et al., 2004). They observed that when *Rx* expression was silenced, it

caused an eyeless phenotype in both species. When performing an *in-situ* hybridization to investigate the expression of genes related to eye formation, *Otx2, Six3, Pax6* and *FoxE3*, in *Rx -/-* mice, they found that the initial activation of *Otx2, Six3 and Pax6* in the anterior neural plate was not *Rx* dependent. The specific upregulation of these genes in the retinal progenitor cells was however found to be *Rx* dependent. *FoxE3*, an early marker of lens development was not detected either, proving that *Rx* is essential for vertebrate eye formation (Bailey et al., 2004). By combining their results with data from several studies on other vertebrate species, such as Zebrafish, chick and medaka, they proposed a simple regulatory network for *Rx* (Bailey et al., 2004; Casarosa et al., 2003; F. Loosli et al., 2001; Felix Loosli et al., 2003; Mathers et al., 1997; Ohuchi et al., 1999). *Otx2* transcription is turned on in the anterior neuroectoderm with the inhibition of Wnt and Nodal. *Otx2* then activates transcription of *Rx*. *Rx* promotes proliferation and performs several functions required for the formation of retinal progenitor cells. *Rx* then increases the transcription of several genes involved in eye development like *Pax6*, *Six3* and *Lhx2*, while also downregulating the transcription of *Otx2* in the presumptive neuroretina (Bailey et al., 2004).

1.5.1 Diseases related to Retinal homeobox

Mutations to the human *Rx* gene have been linked to several symptoms grouped together under the phenotype "Syndromic microphthalmia-16 "(MCOPS16), OMIM entry #611038 (Amberger et al., 2019). MCOPS16 is characterized by anophthalmia (the absence of one or more eyes) or severe microphthalmia (underdeveloped eye structures). Other characteristic features of MCOPS16 are a variable presence of midline defects such as cleft lip and palate, absence of frontal and/or sphenoidal sinuses, and absent pituitary gland. In some patients developmental delay, intellectual disability or autism can be observed (Amberger et al., 2019; Danno et al., 2008).

1.6 Aims of the study

The vertebrate *Rx* gene has a well-described role in the formation of the retina, and the formation and proliferation of retinal progenitor cells. The function of *NvRx* in *Nematostella* is in contrast not understood yet. In the transcriptomic analysis of the *NvFoxQ2d*::*mOrange*-expressing cells, it was found that *NvRx* is highly upregulated in this cell population. The working hypothesis for this thesis was that *NvRx* might play a role in the development of this population, either as a regulator of *NvFoxQ2d*, or as a regulatory target for *NvFoxQ2d*.

The aim of this study was therefore to (1) characterize the expression pattern of *NvRx* at an improved temporal resolution and in relation to *NvFoxQ2d* and other neural genes, and to (2) determine the

function and regulatory network of *Rx* in *Nematostella.* To achieve aim 1, an *in-situ* hybridization (ISH) was performed using a 1419bp *Rx* probe on wild-type animals. To test if *NvRx* co-localizes with *NvFoxQ2d,* a double fluorescence *in-situ* hybridization (FISH) was performed*.* To achieve aim 2, *NvRx* short hairpin RNA (shRNA) was injected into fertilized wild type (WT) eggs. The animals were then raised to gastrula and planula stages where *in-situ* hybridizations were performed looking for changes in expression of other genes found upregulated in the *NvFoxQ2d::mOrange* transcriptome*.* A mutant knockout line was also generated using CRISPR/Cas9 to investigate the function of *NvRx* in *Nematostella* beyond the stages affected by knockdown injections.

2 Materials

2.1 Chemicals

Chemical	Formula/Abbreviation	Supplier	Cat. no
4',6-Diamidino-2-phenylindole	DAPI	Thermo Fisher	62248
Acetic Anhydride	$(CH_3CO)_2O$	Sigma Aldrich	320102
Agarose	-	Invitrogen	16500100
Bisbenzimide	Hoechst 33342	Thermo Fisher	62249
Bovine serum albumin	BSA	Sigma Aldrich	A7906
Chloroform	$CHCl_3$	Sigma Aldrich	372978
Citric acid	$C_6H_8O_7$	Sigma Aldrich	C0759
di-Sodium hydrogen phosphate dihydrate	Na_2HPO_4 x 2 H_2O	Sigma Aldrich	71643
Ethanol	CH_3CH_2OH /EtOH	Supelco	1.00983
Ethylenediaminetetraacetic acid	EDTA	Sigma Aldrich	E6758
Formaldehyde	CH_2O	Sigma Aldrich	252549
Formamide	CH_3NO	Sigma Aldrich	F9037
Glutaraldehyde	$C_5H_8O_2$	Sigma Aldrich	G7651
Glycerol	$C_3H_8O_3$	Sigma Aldrich	G5516
Glycine	$C_2H_5NO_2$	Sigma Aldrich	50046
Heparin sodium salt	-	Sigma Aldrich	H3149
Hydrogen peroxide	H_2O_2	Supelco	1.07209
L-Cysteine	$C_3H_7NO_2S$	Sigma Aldrich	W326305
Lithium Chloride	LiCl	Invitrogen	AM9480
Magnesium chloride hexahydrate	$MgCl_2$ x $6H_2O$	Supelco	1.05833
Maleic Acid	$C_4H_4O_4$	Sigma Aldrich	M0375
Methanol	CH_3OH / MeOH	Sigma Aldrich	32213-M
Nitro-blue tetrazolium chloride/5-bromo-4-chloro-3'-indolyphosphate p-toluidine salt	NBT/BCIP	Roche	11681451001
Polyethylene glycol sorbitan monolaurate	Tween20	Sigma Aldrich	P9416
Potassium chloride	KCl	Sigma Aldrich	P9541
Proteinase K	-	Sigma Aldrich	P2308
Sodium Chloride	NaCl	Sigma Aldrich	S9888
Sodium citrate tribasic dehydrate	Na citrate	Supelco	1.6448
Sodium dihydrogen phosphate monohydrate	NaH_2PO_4 x H_2O	Sigma Aldrich	71504-MM
Sodium dodecyl sulfate	$CH_3(CH_2)_{11}OSO_3Na$ / SDS	Sigma Aldrich	05030
Sodium hydroxide	NaOH	Supelco	1.06462
t-Octylphenoxypolyethoxyethanol	Triton X-100	Sigma Aldrich	T8787
Triethanolamine	$C_6H_{15}NO_3$ / TEA	Sigma Aldrich	90278
Tris-HCl	$NH_2C(CH_2OH)_3$ x HCl	Sigma Aldrich	T5941
Tris-acetate	$NH_2C(CH_2OH)_3$ x CH_3COOH	Sigma Aldrich	93337

2.2 Buffers and solutions

10x PBS

18.6mM NaH_2PO_4 x H_2O
84.1mM Na_2HPO_4 x 2 H_2O
1.75M NaCl

20x SSC (pH7.0)

3M NaCl
300mM NaCitrate

1x PBTw	**1x PBTx**	**2x SSCT**	**0.5x SSCT**
1x PBS	1x PBS	10% (v/v) 20x SSCT	0.5% (v/v) 20x SSCT
0.1% (v/v) Tween20	0.2% (v/v) Triton X-100	0.4%(v/v) Tween20	0.4% (v/v) Tween20

TNTw	**TNTx**	**1x Maleic acid buffer (MAB, pH 7.5)**
100mM Tris-HCl (pH7.5)	100mM Tris-HCl (pH7.5)	100mM Maleic acid
150mM NaCl	150mM NaCl	150mM NaCl
0.1% (v/v) Tween20	0.2% (v/v) Triton X-100	

Hybridization buffer (+) / Hyb(+)	**Hybridization buffer (-) / Hyb (-)**
50% (v/v) Formamide	50% (v/v) Formamide
5x SSC	5x SSC
1% SDS	1% SDS
0.1% Tween20	0.1% Tween20
9.25mM Citric acid	9.25mM Citric acid
50µg/mL Heparin	
100µg/mL Salmon sperm DNA	

Blocking buffer for FISH	**Blocking buffer for ISH**
100mM Tris-HCl (pH7.5)	1x Maleic acid buffer
150mM NaCl	10% (w/v) Boehringer Blocking solution
0.5% (v/v) TSA® Plus Blocking	

TAE buffer	**PBS-Tx-BSA**
40mM Tris-acetate	1x PBS
1mM EDTA	0.2% (v/v) Triton X-100
TAE buffer	0.1% (w/v) BSA

DNA extraction buffer	**NTMT**
10mM Tris-HCl (pH8.0)	100mM Tris-HCl (pH9.5)
1mM EDTA	100mM NaCl
25mM NaCl	50mM $MgCl_2$
200µg/µl Proteinase K	0.1% (v/v) Tween20

2.3 Commercial kits and reagents

Chemical	Supplier	Cat. no	Application
Alexa488 Dextran	Thermo Fisher	D22910	Injection
Boehringer Blocking solution	Roche	11096176001	Blocking for ISH
dNTPs	Thermo Fisher	R0194	PCR
Deoxyribonucleic acid, single stranded from salmon testes	Sigma Aldrich	D9156	Hybridization buffer
Cas9	PNABio	CP01	CRISPR injection
EnGen sgRNA synthesis kit	EnGen	E3322 S	sgRNA synthesis
EvaGreen	Biotium	#31000	Melt curve
Gel Loading Solution	Sigma Aldrich	G7654	Agarose gel electrophoresis
GeneRuler DNA Ladder Mix	Thermo Fisher	SM0331	Agarose gel electrophoresis
High-Capacity cDNA Reverse Transcription Kit	Thermo Fisher	4368814	qPCR
MassRuler Low Range DNA Ladder	Thermo Fisher	SM0383	Agarose gel electrophoresis
PowerUp™ SYBR™ Green Master Mix	Thermo Fisher	A25741	qPCR
ProLong Gold	Thermo Fisher	P36930	FISH slide mounting
RNeasy® Mini Kit	Qiagen	74104	qPCR
SYBR Safe® DNA gel stain	Invitrogen	S33102	Agarose gel electrophoresis
TSA® Plus Blocking	PerkinElmer	FP1012	Blocking for FISH
TSA® Plus Cyanine 3	PerkinElmer	NEL744001KT	FISH staining
TSA® Plus fluorescein	PerkinElmer	NEL741001KT	FISH staining
TRIzol	Invitrogen	15596018	qPCR
Q5® High-Fidelity DNA Polymerase	NEB	M0491	PCR
Q5® Reaction Buffer	NEB	B9027	PCR

2.4 Antibodies

Name	Supplier	Cat. no	Species	Dilution
Anti-Digoxigenin-AP	Roche	11093274910	Sheep	1:4000
Anti-Digoxigenin-POD	Roche	11207733910	Sheep	1:100
Anti-Dinitrophenol-HRP	PerkinElmer	FP1129	Unspecified	1:250

2.5 Instruments

Name	Supplier	Function
CellTram® vario	Eppendorf	Microinjection
CFX Opus 96 Real-Time PCR System	Bio-Rad	qPCR
Nikon Eclipse TE2000-U	Nikon	Microinjection
Eppendorf Mastercycler® nexus SX1 Thermal Cycler	Eppendorf	PCR
FemtoJet® 4i	Eppendorf	Microinjection
Gel Doc EZ System	Bio-Rad	Gel imaging
LightCycler®480	Roche	Melt curve analysis
Nikon Digital Sight DS-U3	Nikon	ISH imaging
Nikon Eclipse E800	Nikon	ISH imaging
Nikon Intensilight C-HGFI	Nikon	ISH imaging
Olympus Fluoview FV3000	Olympus	FISH imaging
P-97 FLAMING/BROWN	Sutter instrument	Micropipette puller

2.6 Computer software

Name	Producer	Version	Purpose
LightCycler®480 software	Roche	v1.5.1.62	qPCR/Melt curve
CFX Maestro	Bio-Rad	v2.3	qPCR
FV31S-SW	Olympus	v2.4.1.198	FISH imaging
ImageJ	National Institutes of Health	v1.53t	Image visualization and manipulation, Figure creation
Image Lab	Bio-Rad	v5.1	Gel imaging
NIS Elements	Nikon	v5.11.01	Colorimetric *In-situ* imaging
Photoshop	Adobe	CS5 v12.0	Image visualization and manipulation, Figure creation
PyMol	Schrödinger LLC	v2.5.2	PDB file visualization
RStudio	Posit Software, PBC	2022.12.0 Build 353	Data analysis and visualization

2.7 Probes

Probe	Accession number	Purpose
Rx probe	HM004556 (Source: (Mazza et al., 2010))	*In-situ* hybridization
FoxQ2d probe	KY292414 (Source: (Busengdal & Rentzsch, 2017))	*In-situ* hybridization
Rfx4 probe	NVE7731 (Source: (Fredman et al., 2013))	*In-situ* hybridization
PaxC probe	AY730691 (Source: (Matus et al., 2007))	*In-situ* hybridization
Elav1 probe	LT795588 (Source: (Steinmetz et al., 2017))	*In-situ* hybridization
SoxB2 probe	DQ173696 (Source: (Magie et al., 2005))	*In-situ* hybridization
RFamide probe	NVE7549 (Source: (Fredman et al., 2013))	*In-situ* hybridization
Mucin probe	LT795565 (Source: (Steinmetz et al., 2017))	*In-situ* hybridization

2.8 Primers

Primer	Sequence 5' - 3'	Purpose
Exon1-Guide1 sgRNA	ttctaatacgactcactata**G**CTAATATGGCATCGATTGAGgttttagagctaga *	CRISPR/Cas9
Exon1-Guide2 sgRNA	ttctaatacgactcactata**G**CGACTCCAACCCAAGACTAGgttttagagctaga *	CRISPR/Cas9
Exon2-Guide1 sgRNA	ttctaatacgactcactataGTGTAACTGAAACGTTGTGAgttttagagctaga *	CRISPR/Cas9
Exon2-Guide2 sgRNA	ttctaatacgactcactata**G**TGGATAGTGGGATTTCTCGAgttttagagctaga *	CRISPR/Cas9
Exon2-Guide3 sgRNA	ttctaatacgactcactata**G**TGTGTACACGTCTGGATAGTgttttagagctaga *	CRISPR/Cas9
Exon1-Guide1 Fwd primer	GGAGATAGTCAGTCTGAAGCC	Melt curve analysis
Exon1-Guide1 Rev primer	CCAGAACAAGAGCGAAAGACTA	Melt curve analysis
Exon1-Guide2 Fwd primer	CCAGAACAAGAGCGAAAGACTA	Melt curve analysis
Exon1-Guide2 Rev primer	GATTTGAGCTCCAACGATGG	Melt curve analysis
Exon2 Fwd primer	GCTCAGAAGAAACCGTACCA	Melt curve analysis
Exon2 Rev primer	CTCCCTGAAGTTAGGGTACA	Melt curve analysis
Deletion Fwd primer	CACATCGCGCAAGTATGAGC	Gel electrophoresis
Deletion Rev primer	AACGGCTTCACTCTTGACCC	Gel electrophoresis
Rx sense shRNA	taatacgactcactataGGAGCTCAAATCATTGTCTttcaagagaAGACAATGATTTGAGCTCCtt **	shRNA injection
Rx antisense shRNA	aaGGAGCTCAAATCATTGTCTtctcttgaaAGACAATGATTTGAGCTCCtatagtgagtcgtatta **	shRNA injection
GFP sense shRNA	taatacgactcactataGTGGAGTTGTAAGGAGCTGTttcaagagaACAGCTCCTTACAACTCCACtt **	shRNA injection
GFP antisense shRNA	aaGTGGAGTTGTAAGGAGCTGTtctcttgaaACAGCTCCTTACAACTCCACtatagtgagtcgtatta **	shRNA injection
ATPsynt Fwd primer	TGCTGGGAAAGTTCTGGACCAATG	qPCR housekeeping
ATPsynt Rev primer	ACACCCTCCTTGACGGTAACATTC	qPCR housekeeping
EF1b Fwd primer	TGCTGCATCAGAACAGAAACCTGC	qPCR housekeeping
EF1b Rev primer	TAAGCCTTCAAGCGTTCTTGCCTG	qPCR housekeeping
Rx Fwd primer	CAACCCAAGACTAGAGGAAGACG	qPCR gene of interest
Rx Rev primer	GAAACGTTGTGAAGGTGGTACG	qPCR gene of interest
FoxQ2d Fwd primer	CAGAGCTCTACACGCGATACGGAC (Source: (Busengdal & Rentzsch, 2017))	qPCR gene of interest
FoxQ2d Rev primer	GCAGAGCCTTCAGTCGACCAC (Source: (Busengdal & Rentzsch, 2017))	qPCR gene of interest
PaxC Fwd primer	GTTGGATCATAGCTGCTGATCATAGAGC	qPCR gene of interest
PaxC Rev primer	GGTCTGGTTTTCAAATCGACGAGC	qPCR gene of interest
Rfx4 Fwd primer	TGGAAAGATCATAAGGCACACTTTTCC	qPCR gene of interest
Rfx4 Rev Primer	GCCGGAAGAGCTTTGTCTTGC	qPCR gene of interest

* Upper-case letters represent the target-specific sequence.

Bold letters indicate Guanine inserted for stability

Lower-case letters represent T7 promoter (5' end) and Cas9 scaffold complementary overlap (3' end)

** Upper-case letters represent the target-specific sense and antisense sequence.

Lower-case letters represent:

Sense: Polymerase promotor region (5' end), loop structure, overhang (3' end)

Antisense: Polymerase promotor region (3' end), loop structure, overhang (5' end)

3 Methods

3.1 *Nematostella vectensis* husbandry

Animals were housed at 21°C in 1/3 filtered sea water with salinity of 12-14ppt and pH 8.0 (*Nematostella vectensis* medium; NV medium) until sexual maturity to promote accelerated growth. Crushed artemia was used as feed 2 weeks after fertilization until animals were big enough to consume whole artemia. Feeding was performed Monday through Thursday with daily changes of NV medium. Glass beakers containing the animals were washed on Fridays. At sexual maturity, the animals were transferred to the animal facility where they were housed at a constant 18°C.

Gametogenesis was induced by exposure to light and elevated temperatures as described in Fritzenwanker and Technau (Fritzenwanker & Technau, 2002)**.** Egg packages were fertilized at ~16°C for 20-25min before de-jellying for injection.

A de-jellying solution consisting of 3% (w/v) L-Cysteine in NV medium was prepared and adjusted to pH 7.4-7.6 using 1M NaOH. The fertilized egg packages were placed in the de-jellying solution and shaken at 65-70 rpm for approximately 17min with occasional agitation of the packages. To fully remove the cysteine, the eggs were washed by moving them through 5 dishes containing NV medium.

3.2 Injection

Injection needles were pulled in a P-97 Flaming/Brown Micropipette Puller. Settings on the FemtoJet 4i were injection pressure of 250hPa, injection time of 0.47s, and compensation pressure of 15hPa.

3.2.1 shRNA injection

2μL Alexa488/1.1M KCl was added to a 2μL 1800ng/μL shRNA aliquot and mixed by flicking. 3μL shRNA solution was loaded in the injection needle, the tip of the needle was broken using the microcapillary and air was pushed out until Alexa488/shRNA solution came out. Injections of 300 eggs were performed for both *NvRx* shRNA and *GFP* shRNA. The embryos were washed in NV medium to remove contaminations from injection, then raised at 21°C.

3.2.2 CRISPR injection

3μL Cas9/sgRNA solution was loaded in the injection needle, the tip of the needle was broken using the microcapillary and air was pushed out. Injections of roughly 200±50 eggs were performed for each sgRNA. The embryos were washed in NV medium to remove contaminations from injection, incubated at 25°C overnight to optimize Cas9 activity, then subsequently raised at 21°C. See section 3.5 for generation of sgRNAs.

3.3 *In-situ* hybridization

To examine the expression pattern of *NvRx* and other target genes, *in-situ* hybridization was performed. WT embryos were injected with *NvRx* shRNA and *GFP* shRNA as a control, then fixed at 30 and 48hpf. A fluorescence ISH was performed to test the hypothesis that *NvRx* co-localizes with *NvFoxQ2d*. A fluorescence ISH was also performed to see if *NvRx* co-localizes with *NvElav1*.

The ISH samples are hybridized with specific digoxigenin (DIG) labelled probes. Anti-DIG antibodies coupled to alkaline phosphatase (AP) are then bound to the DIG probes, and AP activity can be detected by the addition of 5-bromo-4-chloro-3-indolyl phosphate (BCIP) and nitroblue tetrazolium salt (NBT), creating a purple colour at the probe location (Kessler, 1994). For fluorescence ISH, specific dinitrophenol (DNP) and specific DIG labelled probes were used. Anti-DNP antibodies bound to Horseradish Peroxidase (HRP) and Anti-DIG antibodies bound to Peroxidase (POD) were bound to their respective probes, and the signal was developed using Cyanine3 (Cy3) and Fluorescein.

3.3.1 Fixation

Injected embryos were fixed at 30hpf and 48hpf using 0.2% glutaraldehyde, 3.7% formaldehyde in NV medium for 90sec. Fixation media was replaced by with a weaker fixation media containing cold 3.7% formaldehyde in 1x PBTw, then incubated shaking at 4°C for 1hr. Fixed embryos were washed 3 times in 1x PBTw, once in 1x PBS, once in ddH$_2$O and stored in MeOH at -20°C until further use.

3.3.2 Rehydration, proteinase K treatment and refixation

For fluorescence ISH, a 20min H$_2$O$_2$ treatment was performed using 3% H$_2$O$_2$ in MeOH to stop native peroxidase activity. Rehydration of fixed embryos was done by a series of 5min washes using decreasing amounts of MeOH (75%, 50%, 25%) in 1x PBTw. Three 5min washes in 1x PBT were performed before embryos were transferred to washing baskets and placed in a washing box. The embryos were treated for 5min using 10µg/mL proteinase K in 1x PBTw. The proteinase K was deactivated by two 5min washes, shaking, using 4mg/mL glycine in 1x PBTw. Embryos were treated to prevent unspecific probe binding, using 1% TEA in 1x PBTw for 5min, then 5min using 1% TEA and 0.25% acetic anhydride in 1x PBTw, then 5min using 1% TEA and 0.5% acetic anhydride in 1x PBTw. Embryos were washed three times for 5 min in 1x PBTw before a re-fixation in 3.7% formaldehyde in 1x PBTw for 30min was performed. Five 5min washes were performed using 1x PBTw to remove residual formaldehyde.

3.3.3 Pre-hybridization and hybridization

333µL 60°C HYB(+) was added to each well in a tube rack and the baskets containing the samples were added. Pre-hybridization was performed in the HYB(+) buffer overnight in a 60°C water bath. 1ng/µL

(f.c.) probes were denatured in HYB(+) buffer at 90°C for 5min, cooled to 60°C before 333μL was added to new wells in the tube rack. Baskets were transferred from HYB(+) buffer to their corresponding probes then incubated for >60hrs in a 60°C water bath.

3.3.4 Post-hybridization washes

The embryos were washed for 5min in 60°C 100% HYB(-) buffer (50% formamide, 5x SSC, 1% SDS, 0.1% Tween20 and 9.25mM citric acid) before a series of 30min washes at 60°C were performed with decreasing amounts of HYB(-) buffer (75%, 50%, 25%, 0%) in 2x SSCT (2x SSC, 0.1% Tween20). 20 min washes were performed in 0.2x SSCT (0.2x SSC, 0.1% Tween20) and twice in 0.1x SSCT (0.1x SSC, 0.1% Tween20). At room temperature (RT), a series of 10 min washes was performed in decreasing amounts of 0.1x SSCT (75%, 50%, 25%) in 1x PBTw. The protocol for ISH and FISH differs after post-hybridization washes.

3.3.5 ISH blocking and antibody incubation

Two 5min washes with 1x PBTw were performed before blocking. Blocking was performed using 50/50 (v/v) of 1% Roche blocking solution/MAB (100mM Maleic acid, 150mM NaCl, pH7.5) in 1x PBTw for 5min, then 1% Roche blocking solution/MAB for >2hr. Blocking solution was replaced by 1:4000 (v/v) Anti-DIG-AP in 1% blocking solution and incubated overnight at 4°C. Blocking solution was removed, and embryos were given a quick wash in PBTx-BSA (1x PBS, 0.2% Triton X100 and 0.1% (w/v) BSA) before ten 15min washes were performed in PBTx-BSA.

3.3.6 Development of Alkaline Phosphatase signal

Embryos were washed three times in NTMT (100mM Tris pH9.0, 100mM NaCl, 50mM $MgCl_2$ and 0.1% Tween20) before being stored in NTMT overnight at 4°C. Staining was developed using 1:100 (v/v) NBT/BCiP in NTMT until signal was verified under microscope. After staining, embryos were washed twice in NTMT, twice in PBTw, once PBS, then stored in glycerol at 4°C.

3.3.7 FISH blocking and antibody incubation

Four 5min washes in TNTw (0.1M Tris-HCl pH7.5, 0.15M NaCl, 0.1% Tween20) were performed before blocking. Blocking was performed using 0.5% Perkin Elmer blocking reagent in TNB (0.1M Tris-HCl pH7.5, 0.15M NaCl) for 1hr. Blocking solution was replaced by 1:250 anti-DNP-HRP in 0.5% blocking solution and incubated overnight at 4°C. The antibody solution was removed, and embryos were given ten 15min washes in TNTx (0.1M Tris-HCl pH7.5, 0.15M NaCl, 0.2% Triton X100).

3.3.8 Development of Peroxidase signal

A 1:50 dilution of Cy3 in Perkin Elmer working solution was added to each sample and incubated for 30min in the dark. Three 5min washes in TNTx were performed before Peroxidase (POD) activity was stopped in a 10min incubation in the dark using 0.1M glycine and 0.1% Tween20 adjusted to pH 2.0. Three 5min washes in TNTx was performed before a 1hr block was performed in the dark using 0.5% Perkin Elmer blocking reagent in TNT. Blocking solution was replaced by 1:100 anti-DIG-POD in 0.5% blocking solution and incubated overnight in the dark. The antibody solution was removed, and the embryos were given ten 15min washes in TNTx. A 1:50 dilution of Fluorescein in Perkin Elmer working solution was added to each sample and incubated for 30min in the dark. Samples were washed twice in TNTx, once briefly in PBTx (0.2% (v/v) Triton X100 in 1x PBS) then twice in PBTx for 10min. Samples were stained in 1:1000 DAPI in PBTx for 30min, then washed twice for 10min in PBTx. Samples were moved into a Glycerol solution and 2 drops ProLong Gold was added. Samples were stored at 4°C before mounting.

3.3.9 Imaging

ISH samples were mounted on a microscope slide, then imaged at 20x magnification using Nikon Eclipse E800 and Nikon Digital Sight DS-U3. Both transverse and surface images were taken. FISH samples were mounted, then imaged at 40x magnification using the Olympus Fluoview FV3000 system. DAPI emissions were imaged at 430-470nm, Fluorescein emissions were imaged at 500-540nm and Cy3 emissions were imaged at 570-620nm. Z stacks of FISH images were created using Fiji. Reduced Z stacks were created for areas of interest by limiting the stack size to fewer than 10 slices.

3.4 qPCR

A qPCR was performed using complimentary DNA (cDNA), reverse transcribed from extracted RNA derived from shRNA injected animals, to give quantitative information alongside the ISH data. Using a DNA-specific reporter dye, one can measure DNA amplification by looking at the intensity of fluorescence produced by the dsDNA bound dye. By comparing control samples with injected samples, together with housekeeping genes whose expression remains constant, one can evaluate the change in expression of genes.

3.4.1 RNA extraction

Animals were injected with *NvRx* shRNA and *GFP* shRNA as the control, using the same procedure as for the ISH injections. At 30hpf the animals were transferred to an Eppendorf tube, and in a RNase

free environment, 500µL TRIzol reagent was added to the animals. The sample was then vortexed until the lysis was complete with no visible particles. Samples were then stored at -80°C.

Lysed samples were thawed on ice and then vortexed shortly. 135µL chloroform was added to the samples and vortexed shortly, then incubated for 10min at RT. Phase-separation was performed by spinning the samples at 8000 x g, at 4°C for 10min. The supernatant containing the RNA was extracted, and the precipitate containing proteins and other contaminants was discarded. 300µL 70% EtOH was added and mixed by pipetting. Using the Qiagen RNeasy mini kit, the solution was transferred to a spin column and centrifuged at 8000 x g for 1 min, flow-through discarded. 350µL buffer RW1 was added to the sample and spun down at 8000 x g for 1min, flow-through discarded. 80µL DNase solution was added to the spin-column membrane and incubated for 15min at RT to degrade DNA contaminants. 350µL buffer RW1 was added to the sample and spun down at 8000 x g for 1min, flow-through discarded. 500µL buffer RPE was added to the sample and spun down at 8000 x g for 2min. The spin column was transferred to a new collection tube and spun down at max RPM for 1min. The spin column was transferred to a new collection tube and the RNA was eluted using 30µL nuclease-free water added to the membrane, and the tube was spun down at 8000 x g for 1min. The RNA eluate was put on ice, and a nanodrop measurement was taken. A 1% agarose gel was run to check the integrity of the RNA.

3.4.2 cDNA reverse transcription

Using the High-Capacity cDNA Reverse Transcription Kit, a 2x master mix was prepared on ice, containing 2x RT Buffer, 8mM dNTP mix, 2x RT random primers, 5U Multiscribe™ Reverse Transcriptase and 0.1x RNase inhibitor. 200ng RNA was added to 10µL master mix and mixed by pipetting. The reverse transcription reaction was performed in an Eppendorf Mastercycler® nexus SX1 Thermal Cycler using the settings, 25°C for 10min, 37°C for 120min, 85°C for 5min, then stored at 4°C.

3.4.3 qPCR

A 20µL reaction mix containing 1x PowerUp™ SYBR™ Green Master Mix, 2µL cDNA, 0.5mM qPCR-Fwd primer, and 0.5mM qPCR-Rev primer was produced for each combination of shRNA injected sample and genes of study. The reaction samples were loaded onto a 96-well plate and spun down at 500g. The qPCR was run on CFX Opus 96 Real-Time PCR System using the settings: 50°C for 5min, 92°C for 2min, then 40 cycles of 95°C for 15sec, 64°C for 15sec and 72°C for 1min. Results were exported, and Log2Fold-change values calculated.

3.5 CRISPR/Cas9

A Crispr/Cas9 experiment was performed to create a *NvRx* knockout line of *Nematostella vectensis*. After inducing a double strand break of the DNA using a single guide RNA (sgRNA) and Cas9, the cell will make an attempt to repair the DNA. The hope is for the DNA repair mechanism to make a mistake either by inserting or deleting base pairs causing a frameshift, which could then induce an early stop codon. If this stop codon is induced early enough in the sequence, a non-functional truncated protein will be produced. As the *NvRx* homeobox is located on exons 2 and 3 of the protein, exons 1 and the beginning of exon 2 were targeted to create a truncated version of the *NvRx* protein. The nucleotide sequence at the target site was screened for alterations using Melt-Curve analyses and gel electrophoresis.

3.5.1 sgRNA design

The sgRNA prediction web-tool CRISPOR (Concordet & Haeussler, 2018) was used to design sgRNA guides. The genomic target sequences were submitted using the settings; *Nematostella vectensis* genome (EnsemblMetazoa 76 (GCA_000209225.1) to check for off-target effects, and the Protospacer Adjacent Motif (PAM) setting "20bp-NGG – Sp Cas9, SpCas9-HF1, eSpcCas9 1.1". Suitable sequences in exons 1 and 2 were selected for use. A guanine was placed at the 5' flank of the sequence if the sequence didn't already start with a guanine. Upstream T7 promoter sequence (TTCTAATACGACTCACTATA) was added to the 5' flank of the guide sequence, and Cas9 scaffold binding cite (GTTTTAGAGCTAGA) was added to the 3' flank of the guide sequence before the sequences were ordered.

3.5.2 sgRNA synthesis

A 10µL sgRNA synthesis reaction was prepared for each target oligo using the EnGen sgRNA kit. 1x sgRNA reaction mix, 1µL sgRNA Enzyme Mix, 5mM, 250nM target oligo were mixed by flicking the tube, spun down and incubated at 37°C for 1hr. A control reaction was performed as described above, with the target oligo substituted with 250nM sgRNA Control Oligo. 1µL DNase 1 mix was added to both reactions and incubated at 37°C for 15min. 22µL LiCl was added to the reaction, mixed by pipetting, and stored at -20°C overnight to precipitate the RNA.

The reaction mixture was spun down for 30min at 4°C, 13'500rpm. LiCl was removed carefully by pipetting, leaving the RNA-containing pellet in the Eppendorf tube. 200µL 80% (v/v) EtOH in nuclease-free water was added to wash the pellet before another spin cycle for 15min at 4°C, 13'500rpm. The EtOH was removed, and the pellet was left to air dry for 10 min before being resuspended in 15µL nuclease-free water. A nanodrop measurement was taken before the sgRNA was stored at -80°C.

Table 1: Nanodrop measurements of synthesised sgRNA.

sgRNA	Concentration
Exon1 Guide1	1548 ng/µL
Exon1 Guide2	1013 ng/µL
Exon2 Guide1	1387 ng/µL
Exon2 Guide2	789 ng/µL
Exon2 Guide3	1168 ng/µL
Control	409 ng/µL

3.5.3 Cas9 preparation

A 4µL injection mix containing 1.8µL Cas9, 1µL Alexa488/1.1M KCl and 450ng sgRNA was prepared, mixed by flicking, spun down, and incubated at 37°C for 15min to create the Cas9/sgRNA complex. The injection mixture was stored on ice until injection shortly after.

3.5.4 Genomic DNA extraction

Genomic DNA (gDNA) was extracted from 8 specimens from each sgRNA injected population. The specimens were washed with 180µL absolute EtOH and spun down before most of the EtOH was removed. The samples were incubated at 50°C with the PCR tubes open until all EtOH had evaporated. DNA extraction buffer containing 10mM Tris-HCl (pH 8.0), 1mM EDTA (pH 8.0), 25mM NaCl, and 200µg/µL Proteinase K was added to each sample. The samples were incubated for 2hrs at 50°C, 10min at 90°C then stored at 4°C.

3.5.5 Melt curve analysis

A melt curve analysis was performed on the extracted gDNA to investigate the sgRNA injected lines for possible mutations. PCR was performed using primers flanking the expected mutation sites. The melt curve analysis was then performed on the amplicon using a DNA-specific reporter dye which becomes fluorescent when bound to double stranded DNA. As the temperature increases, the DNA strand dissociates causing the dye to stop fluorescing. The melting temperature of the DNA stand is heavily dependent on the ratio of C/G pairs to A/T pairs, the length and complementarity. By measuring the fluorescence against temperature, one can observe the point of inflection where half of the DNA is denatured.

Melt curve primers were tested to find the optimal run conditions by running PCR programs on WT gDNA samples and subsequently analysed by gel electrophoresis. A 1.4% agarose gel was made by

adding 0.7g agarose to 50mL 1xTAE buffer and 3μL SYBR Safe. Samples were mixed with 6x DNA Gel Loading dye before being loaded on the gel. The gel was run at 90V for 40min, then imaged using a BIO-RAD Gel Doc EZ imager.

A 15μL reaction mix containing 0.2μL Q5 DNA HF DNA Polymerase (2000U/mL), 1x Q5 reaction buffer, 0.33μM dNTPs, 1x EvaGreen, 0.33μM Forward Primer, 0.33μM Reverse Primer and 1μL gDNA from each sample was created. The samples were placed in a Roche LighCycler®480 where 40 cycles of PCR were run at 95°C for 30 seconds, 65°C for 30 seconds, and 72°C for 5 seconds, then a Melt curve analysis was performed from 72°C to 95°C with 0.2°C increments. The data was visualized in RStudio.

Because the change in the genetic sequence of the double guide injected samples was expected to be large, a melt curve analysis was not possible. Instead, PCR and agarose gel electrophoresis was performed. A PCR was first performed using a 15μL reaction mix containing 0.2μL, 2000U/mL Q5 DNA HF DNA Polymerase, 1x Q5 reaction buffer, 0.33μM dNTPs, 0.33μM Forward Primer, 0.33μM Reverse Primer and 1μL gDNA from each sample. The PCR reaction was performed in an Eppendorf Mastercycler® nexus SX1 Thermal Cycler with the same PCR settings as for the melt curve analysis. To detect changes in the size of the target region, the PCR samples were subsequently analysed by gel electrophoresis.

4 Results

The aims for this thesis were to determine the expression pattern of *NvRx* in early development and to investigate the function of *NvRx* in *Nematostella vectensis.* To determine the *NvRx* expression pattern, colorimetric *in-situ* hybridizations were performed on WT embryos. As *NvRx* has been found to be upregulated in the *NvFoxQ2d::mOrange*-expressing cells, fluorescence *in-situ* hybridization was performed to determine if *NvRx* and *NvFoxQ2d* are co-localizing in the same cells. To investigate the function and regulatory networks of *NvRx*, shRNA injections and colorimetric *in-situ* hybridizations were performed. Additionally, several sgRNA's targeting *NvRx* were designed and injected to create CRISPR/Cas9 mediated knockout lines.

4.1 Expression of *NvRx* and *NvSoxB2* at different developmental stages

An *in-situ* hybridization was performed on WT embryos at different stages of development to determine and compare the spatial and temporal expression of transcription factor *NvRx* and neural progenitor marker *NvSoxB2*.

NvSoxB2 was observed to be expressed as early as in the coeloblastula (**Figure 6A**) with expression being present in individual cells distributed over large parts of the blastoderm. In the late blastula stage, cells expressing *NvSoxB2* can be observed mostly on the aboral side of the embryos (**Figure 6B**). In the mid-gastrula stage (**Figure 6C**), we can observe the proceeding of invagination. At this timepoint, expression is limited to the ectoderm, with no expression of *NvSoxB2* observed in the mesendoderm. At late gastrula stage (**Figure 6D**) expression can be observed both in the ectoderm and the forming mesendoderm. In the early planula stage (**Figure 6E**), expression of *NvSoxB2* can be observed throughout the mesendoderm and as scattered cells in the ectoderm. In the mid-planula stage (**Figure 6F**), expression is seen as scattered cells in the ectoderm and mesendoderm. In the late planula stage (**Figure 6G**), *NvSoxB2* expression can observed around the oral opening where tentacle buds are to form in the early polyp stage as well as in scattered cells in the ecto- and mesendoderm.

NvRx expression was observed to start at the mid-gastrula stage (**Figure 6J**), with no observed expression in mid-blastula or late blastula (**Figure 6H-I**). Expression at mid-gastrula is observed as a uniform band in the ectoderm of the aboral half of the animal (**Figure 6J**). No expression was observed in the apical organ region. *NvRx* expression in the late gastrula stage (**Figure 6K**) was observed to be stronger, but still limited to the same area of expression as for mid-gastrula. At early planula stage (**Figure 6L**), individual cells begin to express *NvRx*. Expression can also be observed

expanding to the apical organ region. In the planula stages (**Figure 6M-N**), expression is observed in individual cells throughout the aboral half of the ectoderm.
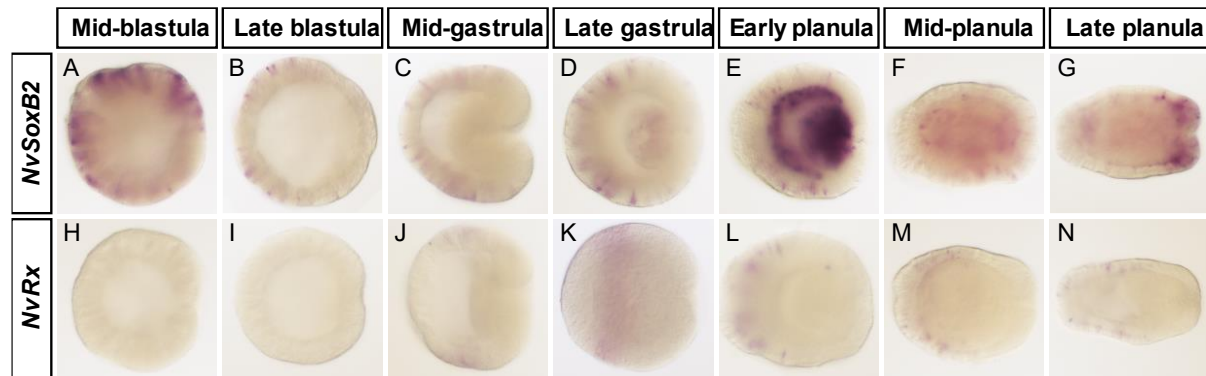

Figure 6: Expression pattern of *NvRx* and *NvSoxB2* in *Nematostella vectensis*. (A-N) *In-situ* hybridization of *NvSoxB2* **(A-G)** and *NvRx* **(H-N)** was performed on seven developmental stages of *Nematostella vectensis* spanning from blastula stage (12hpf) to late planula stage (96hpf) with the orientation aboral pole to the left and oral pole to the right. Images were taken at mid-level, with image **K** being a GFP shRNA injected animal. **(A-G)** Expression of *NvSoxB2* is observed as early as blastula stage (**H**, 12hpf), covering most of the ectoderm. At late blastula (**B**, 16hpf) and mid-gastrula (**C**, 20hpf), individual cells can be observed expressing *NvSoxB2* on the aboral side of the ectoderm. Expression can be observed in the mesendoderm at late gastrula (**D**, 30hpf). In early planula (**E**, 48hpf), expression is observed throughout the mesendoderm and as scattered cells in the ectoderm. Expression can be observed as scattered cells in the ectoderm in mid-planula (**F**, 72hpf) and late planula (**G**, 96hpf). Expression can be observed in the future tentacle buds in the late planula. **(H-N)** No *NvRx* expression was observed at blastula (**H**, 12hpf) or late blastula stage (**I**, 16hpf). Expression was first observed in mid-gastrula (**J**, 20hpf), with expression being observed as a uniform band on the aboral ectoderm. Late gastrula (**K**, 30hpf) expression exhibited the uniform band as mid-gastrula. At early planula stage (**L**, 48hpf), planula stage (**M**, 72hpf) and late planula stage (**N**, 96hpf), expression is observed as scattered cells located mostly on the aboral side of the embryo including the apical tuft region.

4.2 Fluorescence *in-situ* hybridization

To investigate the hypothesis that *NvFoxQ2d* and *NvRx* are expressed in the same cells, double fluorescence *in-situ* hybridization was performed on WT embryos. Three stages of development were investigated: late gastrula (30hpf), early planula (48hpf) and mid-planula stage (72hpf). To investigate if *NvRx*-expressing cells localized to another neural population, a double fluorescence *in-situ* hybridization was performed with the neuronal marker *NvElav1*.

4.2.1 Partial co-expression of *NvFoxQ2d* and *NvRx*.

At 30hpf, very few *NvFoxQ2d*-expressing cells can be observed (**Figure 7A**). *NvRx* is expressed in scattered cells, mostly located on the aboral side of the embryo (**Figure 7B**). Compared to the colorimetric ISH, the signal for *NvRx* appears less homogeneous in FISH at gastrula stage. *When reducing the stack size (i.e. reducing the number of sections in the stack) focusing on the NvFoxQ2d-expressing cells, one can observe co-expression of NvFoxQ2d and NvRx in every NvFoxQ2d-expressing cells* (**Figure 7I**).
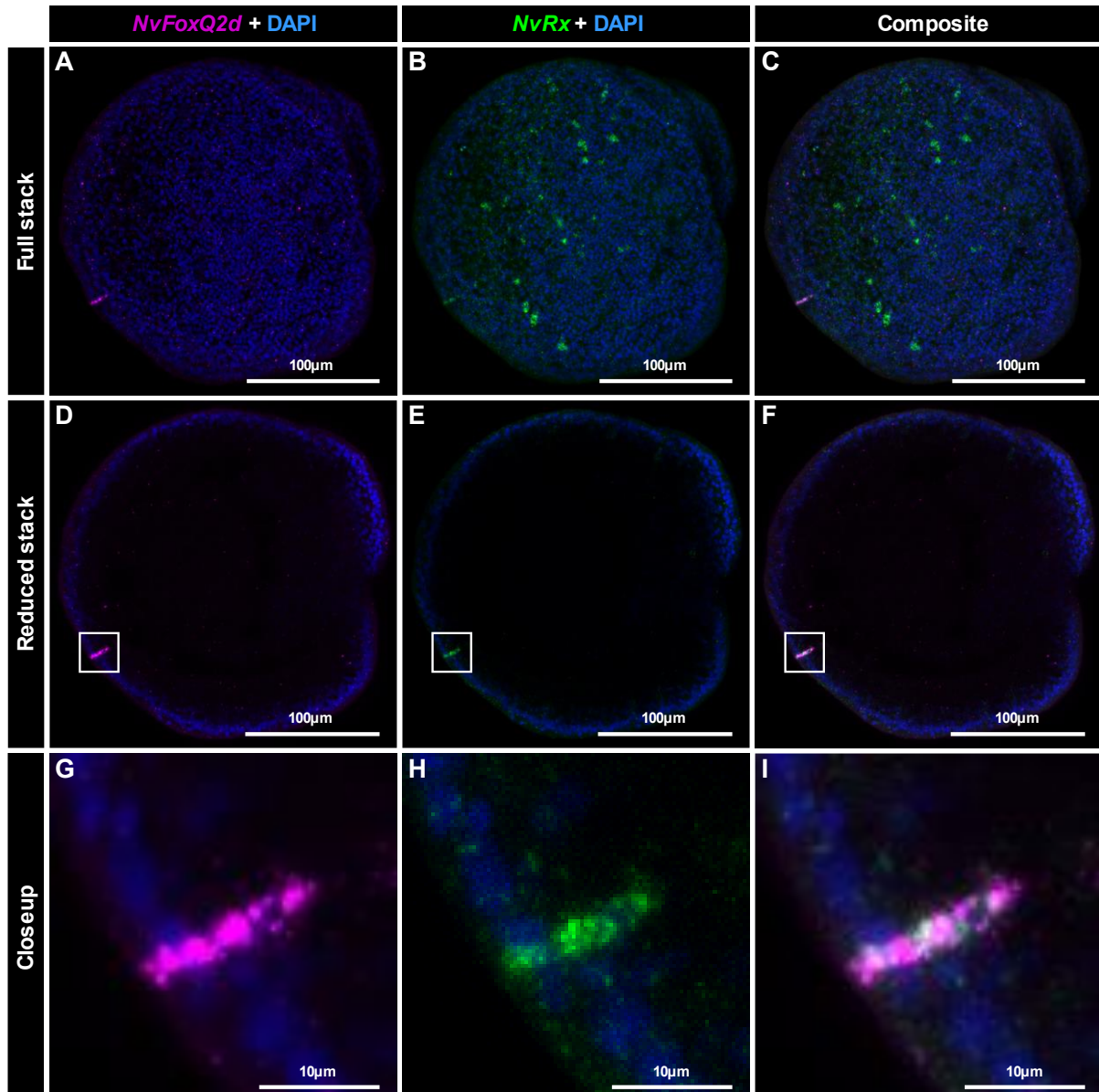
Figure 7: Double fluorescence *in-situ* hybridization of *NvRx* and *NvFoxQ2d* at late gastrula stage (30hfp). Aboral pole is located on the left of the animal and the oral opening is located on the right of the animal. **(A-C)** The full Z-stack shows a handful of scattered *NvRx*-positive cells, and a few *NvFoxQ2d*-positive cells. Most of the observed cells were located on the aboral side of the embryo. **(D-F)** The Z-stack was reduced to show cells within a few slices (<10 slices). **(G-I)** Closeup of the reduced Z-stack reveal co-expression of *NvRx* and *FoxQ2d* in the same cell.

At 48hpf, we can observe a larger amount of *NvFoxQ2d*-positive cells being expressed compared to 30hpf (**Figure 8A**). Expression is observed almost exclusively on the aboral side of the embryo, both for *NvFoxQ2d* and *NvRx* (**Figure 8A-B**). When reducing the stack size, focusing on the *NvFoxQ2d*-positive cells, one can observe co-localization of *NvFoxQ2d* and *NvRx* in most of the cells (**Figure 8C,F,I**). Compared to 30hpf, where every *NvFoxQ2d*-positive cell show co-expression with *NvRx*, one can observe cells only expressing *NvFoxQ2d* at 48hpf (**Figure 8I**).
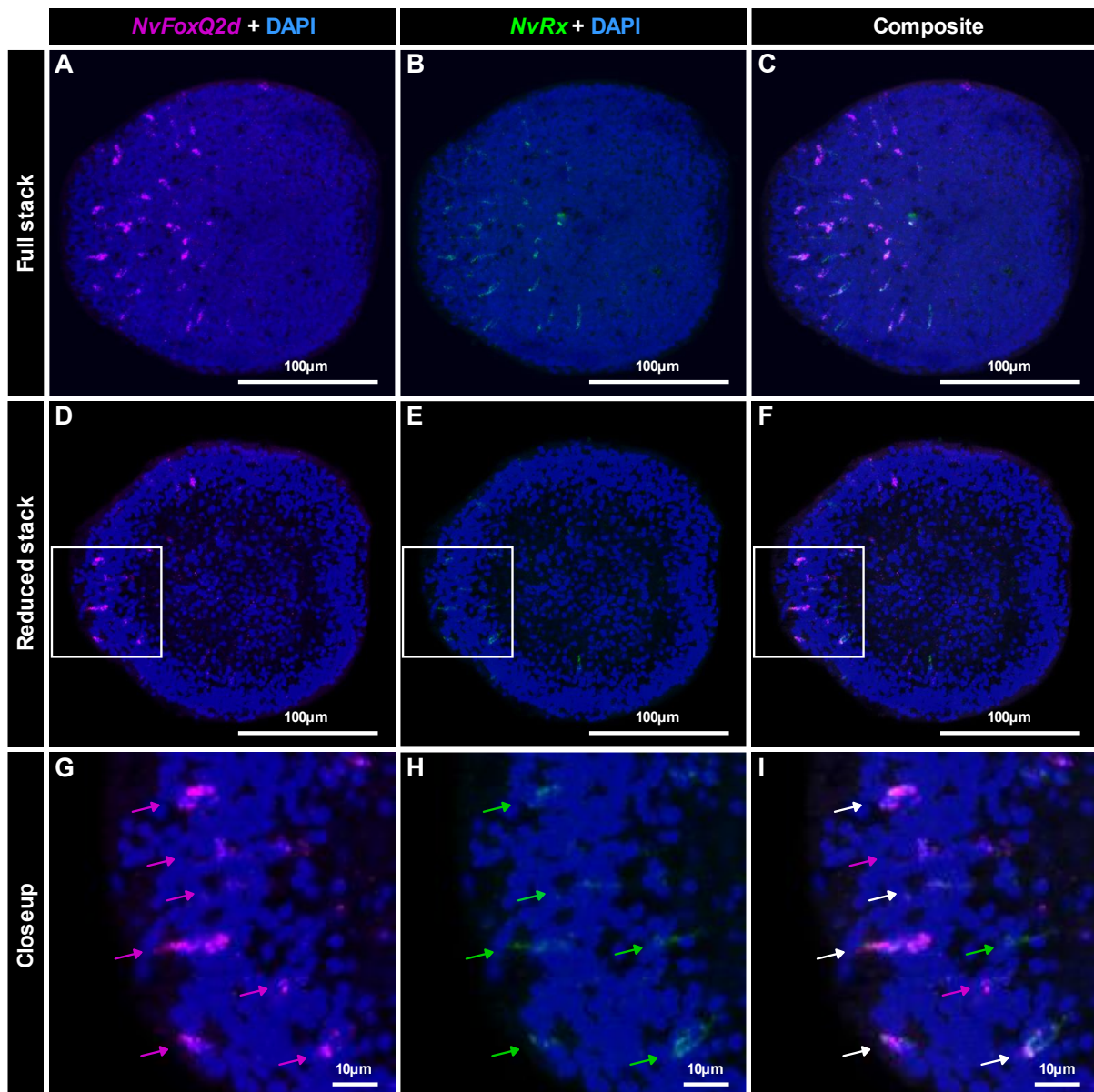
Figure 8: **Double fluorescence *in-situ* hybridization of *NvRx* and *NvFoxQ2d* at early planula stage (48hfp).** Aboral pole is located on the left of the animal and the oral opening is located on the right of the animal. **(A-C)** The full Z-stack shows a scattered expression of *NvRx* and *NvFoxQ2d*-positive cells, with most of the observed cells being located on the aboral side of the embryo. **(D-F)** The Z-stack was reduced to show cells within a few slices (<10 slices). **(G-I)** Closeup of the reduced Z-stack reveal co-expression of *NvRx* and *FoxQ2d* in the majority of the cells observed, indicated with white arrows **(J)**. A few cells, indicated in green or pink, only show expression of one of the two genes.

At 72hpf, we can observe a reduced number of *NvFoxQ2d*-expressing cells compared to 48hpf. Expression is still observed mostly on the aboral side of the embryo for both *NvFoxQ2d* and *NvRx* (**Figure 9A-B**). When reducing the stack size, focusing on the *NvFoxQ2d*-positive cells, one can observe co-localization of *NvFoxQ2d* and *NvRx* in most of the *NvFoxQ2d*-positive cells (**Figure 9I**).
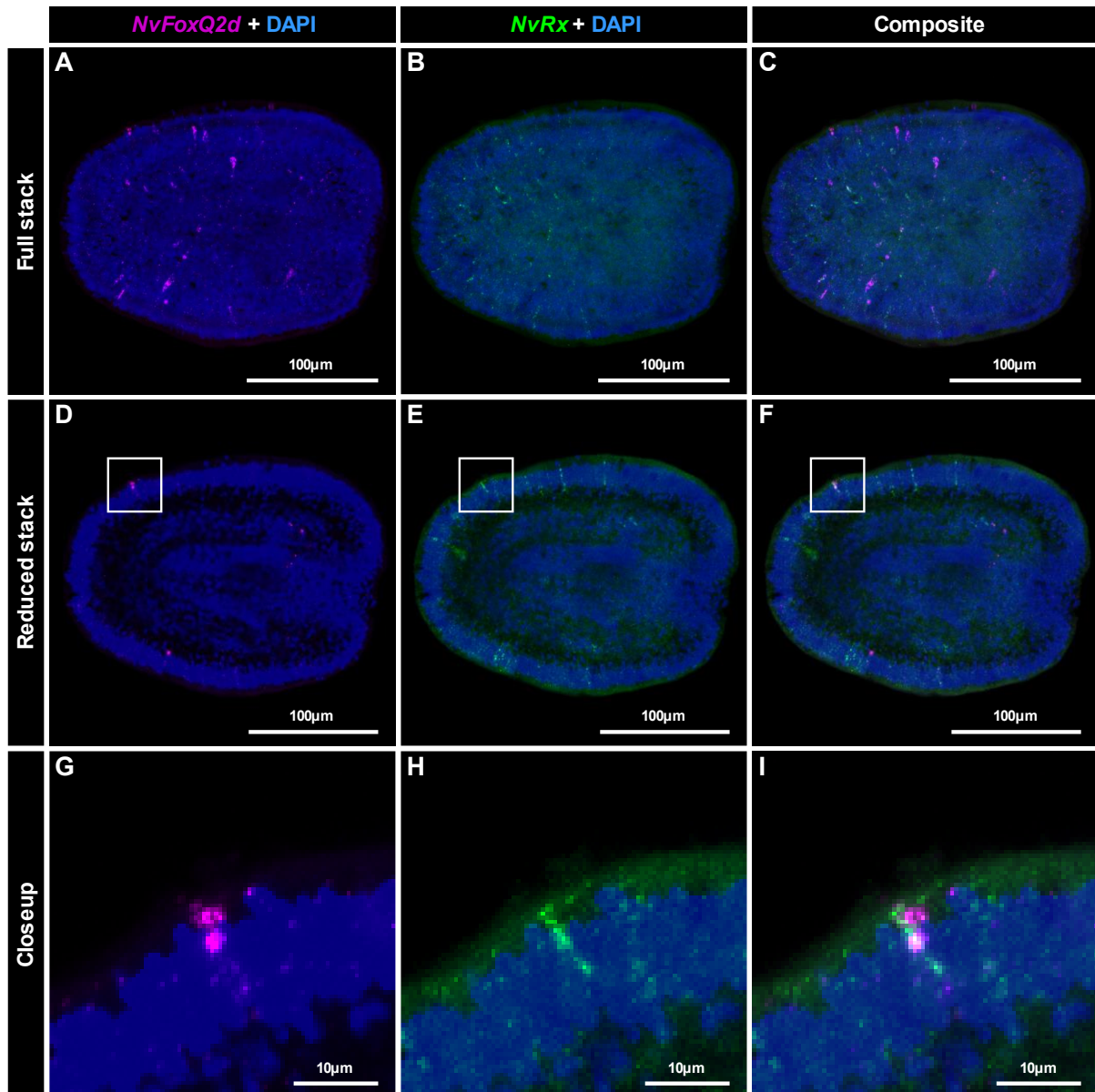
Figure 9: Double fluorescence *in-situ* hybridization of *NvRx* and *NvFoxQ2d* at mid-planula stage (72hfp). Aboral pole is located on the left of the animal and the oral opening is located on the right of the animal. **(A-C)** The full Z-stack shows a scattered expression of *NvRx* and *NvFoxQ2d*-positive cells. **(D-F)** The Z-stack was reduced to show cells within a few slices (<10 slices). **G-I)** Closeup of the reduced Z-stack reveal co-expression of *NvRx* and *FoxQ2d* in the same cell.

4.2.2 NvRx and *NvElav1* are expressed in close proximity.

At 30hpf, very few fluorescent cells could be observed for both *NvRx* and *NvElav1*. Some fluorescent cells are in close proximity to each other, however, no co-expression of *NvRx* and *NvElav1* was observed in any of the samples imaged.
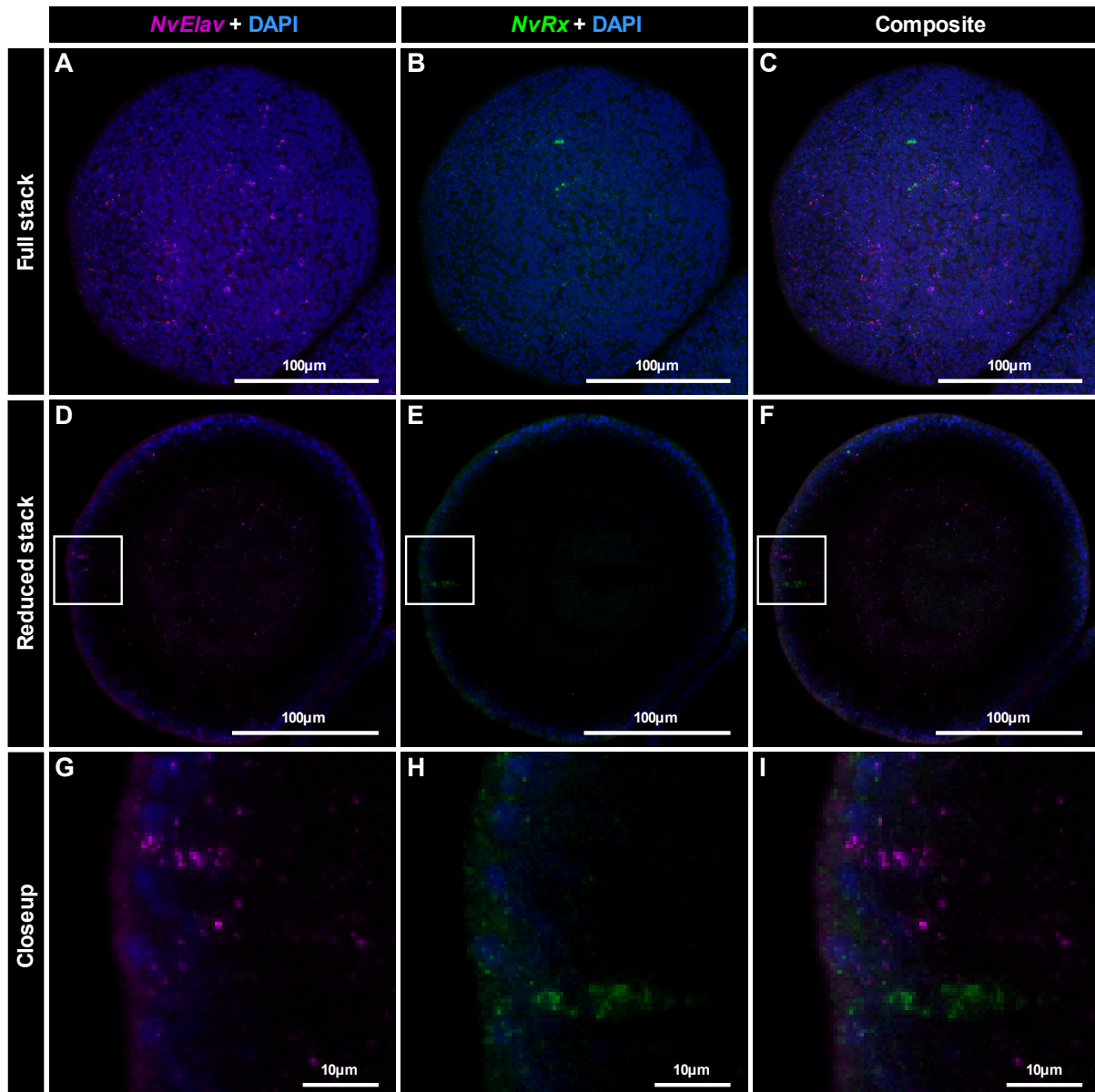
Figure 10: Double fluorescence *in-situ* hybridization of *NvRx* and *NvElav1* at late gastrula stage (30hfp). Aboral pole is located on the left of the animal and the oral opening is located on the right of the animal. **(A-C)** The full Z-stack shows few cells expressing *NvRx* and *NvElav1*. **(D-F)** The Z-stack was reduced to show cells within a few slices (<10 slices). **(G-I)** Closeup of the reduced Z-stack shows *NvRx* and *NvElav1*-positive cells in close proximity to each other. No cell was found co-expressing *NvRx* and *NvElav1*.

At 48hpf, an increased number of *NvElav1* and *NvRx*-positive cells could be observed. *NvRx* was observed to be expressed mostly on the aboral side of the animal, while *NvElav1* expression could be observed throughout the embryo. When reducing the stack size and focusing on the *NvRx*-positive cells, one can observe *NvElav1*-positive and *NvRx*-positive cells being in very close proximity to each other. One cell, indicated with a white arrow (**Figure 11I**), was observed to co-express *NvRx* and *NvElav1*.
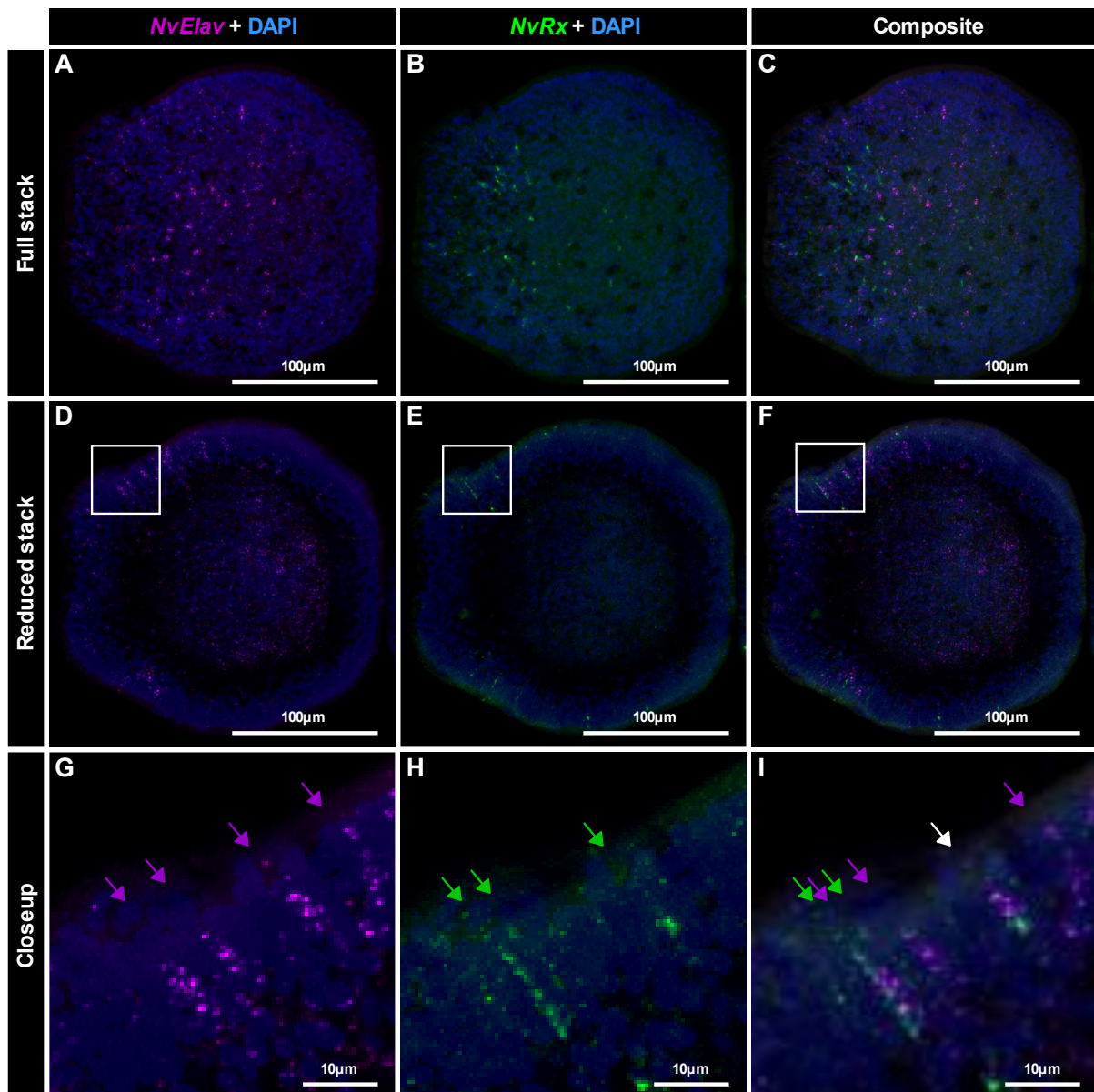
Figure 11: Double fluorescence *in-situ* hybridization of *NvRx* and *NvElav1* at early planula stage (48hfp). Aboral pole is located on the left of the animal and the oral opening is located on the right of the animal. **(A-C)** The full Z-stack shows a handful of scattered cells expressing *NvRx* and *NvElav1*. **(D-F)** The Z-stack was reduced to show cells within a few slices (<10 slices). **(G-I)** Closeup of the reduced Z-stack shows *NvRx* and *NvElav1*-positive cells in very close proximity to each other. One cell was observed to have co-expression of *NvRx* and *NvElav1*, indicated with a white arrow, **(I)**.

At 72hpf, an even greater number of *NvElav1* and *NvRx*-positive cells could be observed. *NvRx* was observed to be expressed mostly on the aboral side of the animal, while *NvElav1* expression could be observed throughout the embryo, both in the mesendoderm and the ectoderm. As with the 48hpf FISH samples, when reducing the stack size one can observe *NvElav1*-positive and *NvRx*-positive cells being in very close proximity to each other.
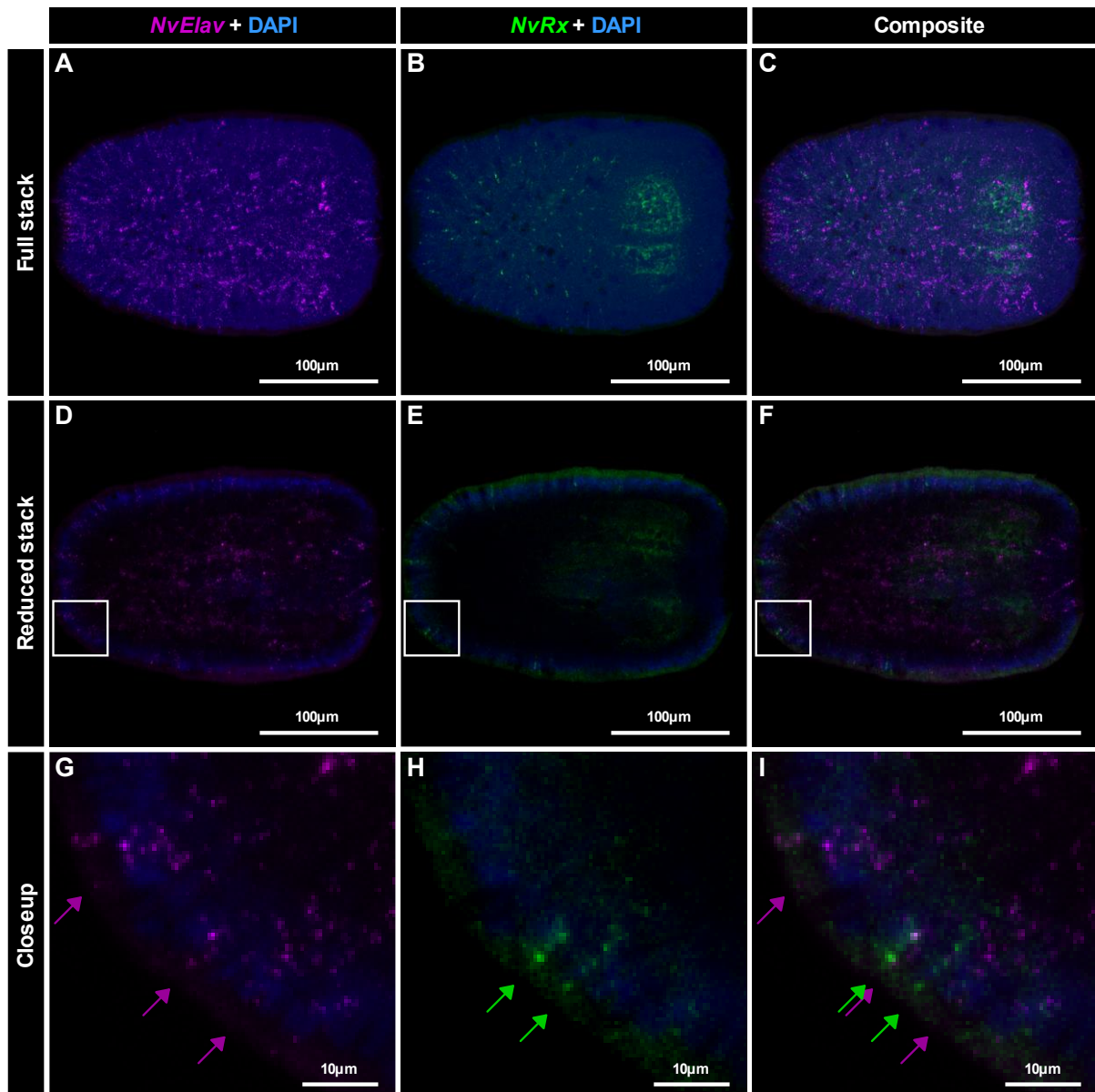
Figure 12: Double fluorescence *in-situ* hybridization of *NvRx* and *NvElav1* at mid-planula stage (72hfp). Aboral pole is located on the left of the animal and the oral opening is located on the right of the animal. **(A-C)** The full Z-stack shows scattered *NvRx*-positive cells, mostly on the aboral side. *NvElav1*-positive cells can be observed across the entire animal. **(D-F)** The Z-stack was reduced to show cells within a few slices (<10 slices). *NvElav1*-expressing cells can be observed both in the ectoderm and mesendoderm. **(G-I)** Closeup of the reduced Z-stack shows *NvRx* and *NvElav1*-positive cells in very close proximity to each other. No cells were observed to have a co-expression of *NvRx* and *NvElav1*.

4.3 *In-situ* hybridization in *NvRx* shRNA injected animals

To determine the function and parts of the regulatory network of *NvRx*, fertilized WT eggs were injected with *NvRx* shRNA (sh*NvRx*) using *GFP* shRNA (sh*GFP*) as the control. The injected embryos were fixed at timepoints 30hpf and 48hpf, and a colorimetric *in-situ* hybridization was performed. The genes investigated were chosen based on a previous transcriptomic analysis of the

NvFoxQ2d::mOrange-positive cells (Gahan, Kouzel, Bartsch, Rentzsch unpublished data). The genes chosen were initially *NvFoxQ2d, NvRfx4* and *NvPaxC.* In addition, genes known to be expressed in neurons (*NvRFamide*), and in secretory cells (*NvMucin*), were included for the 48hpf ISH.

Looking at the *NvRx* expression (**Figure 13A,E,I,M**), one can see that the expression pattern of the sh*GFP* injected samples (**Figure 13A,E**) matches the expression pattern observed in the non-injected samples described in **Figure 13D**. When comparing the sh*GFP* injected samples against the sh*NvRx* injected samples (**Figure 13I,M**), one can see that the *NvRx* expression is completely knocked down in the sh*NvRx* injected samples. *NvFoxQ2d* expression in the sh*GFP* injected embryos is spanning from the midline to the aboral side (**Figure 13B,F**). In sh*NvRx* injected samples (**Figure 13J,N**), *NvFoxQ2d* expression is absent.

Injection of sh*NvRx* did not seem to have an effect on the expression pattern of *NvRfx4*. In the sh*GFP* injected samples (**Figure 13C,G**), one can observe a dense population of *NvRfx4*-expressing cells in the ectoderm, situated mostly on the aboral side, with a few cells observed on the oral side of the embryo. The same expression pattern is observed in the sh*NvRx* injected samples (**Figure 13K,O**).

The expression pattern of *NvPaxC* does not appear to be altered either. Looking at the expression pattern of *NvPaxC* (**Figure 13D,H,L,P**), one can observe a handful of cells scattered across the ectoderm. Comparing the sh*GFP* injected samples with the sh*NvRx* injected samples, no discernible difference in the expression can be observed.
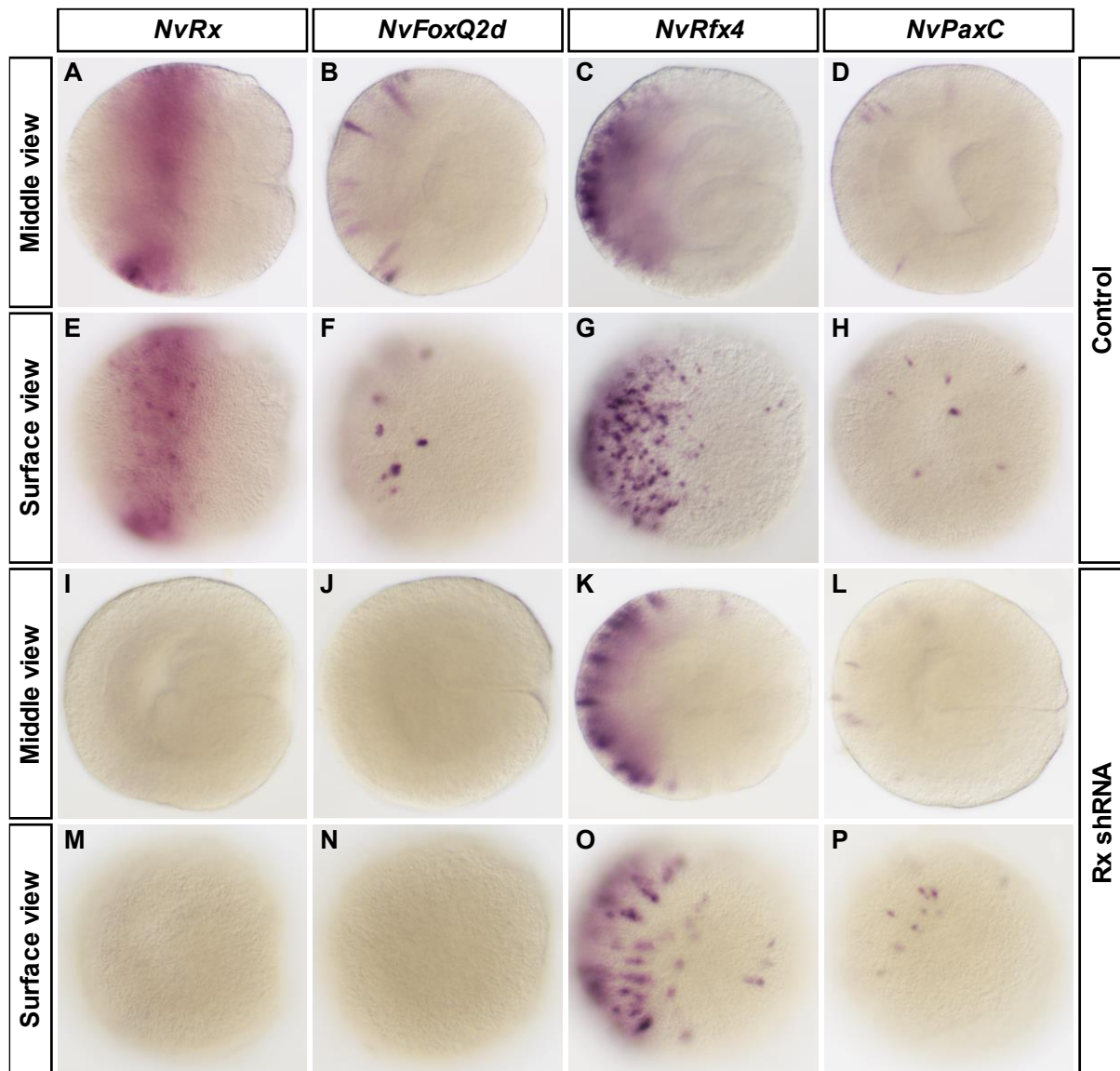
Figure 13: Colorimetric *in-situ* hybridization of late gastrula embryos injected with *NvRx* shRNA and *GFP* shRNA. Aboral pole is located on the left of the animal and the oral opening is located on the right of the animal. **A-H** shows the middle and surface view of sh*GFP* injected embryos. **I-P** shows the middle and surface view of sh*NvRx* injected embryos. **(A-H)**: *NvRx* expression in control samples **(A, E)**, is observed as a mostly uniform band of expression on the middle- to aboral side of the embryo. *NvFoxQ2d* expression in control samples **(B, F)**, is observed as a handful of scattered cells on the aboral side of the ectoderm. *NvRfx4* expression in control samples **(C, G)**, is observed as a dense cluster of cells in the aboral ectoderm of the embryo. Some cells can be observed on the oral side of the animal. *NvPaxC* expression in control samples **(D-H)**, can be observed as a few cells scattered across the ectoderm of the embryo. **(I-P)**: Injection of sh*NvRx* caused a complete silencing of *NvRx* expression **(I, M)**, and of *NvFoxQ2d* **(J, N)**. Injection of sh*NvRx* did not have an effect on either *NvRfx4* **(K, O)** or *NvPaxC* **(L, P)**.

At planula stage, looking at the *NvRx* expression in the sh*GFP* injected samples (**Figure 14A,G**), one can observe the same band of uniform expression that was observed for the late gastrula stage (**Figure 13A,E**). One can also observe scattered individual cells expressing *NvRx*. These cells can be observed across the entire ectoderm, but most are located on the aboral side of the embryo. When comparing the sh*GFP* injected samples against the sh*NvRx* injected samples (**Figure 14M,S**), one can see that the *NvRx* expression is almost completely knocked down. A faint signal can be observed, indicated with

42

black arrowheads, in the aboral side of the embryo. Looking at the *NvFoxQ2d* expression in the sh*GFP* injected samples (**Figure 14B,H**), one can observe scattered cells expressing *NvFoxQ2d* across the entire ectoderm, with the majority of cells located on the aboral side of the embryo. When comparing the sh*GFP* injected samples against the sh*NvRx* injected samples (**Figure 14N,T**), one can see that the *NvFoxQ2d* expression is almost completely knocked down. Some faint cellular expression can be observed, indicated with black arrowheads, in the aboral end of the embryo. No discernible difference in expression of *NvRfx4* or *NvPaxC* can be observed. Comparing the *NvPaxC* expression with the 30hpf ISH, one can observe a larger number of cells being expressed at 48hpf, most of which are located at the aboral pole of the embryo. *NvRFamide* is expressed in a small number of scattered cells in the ectoderm. No change in expression pattern was observed between the sh*GFP* and sh*NvRx* injected embryos. *NvMucin* expression can be observed as a dense cluster of cells on the aboral ectoderm. The density of cells decreases towards the oral side, with a few cells observed in the pharynx. No change in expression was observed between the sh*GFP* and sh*NvRx* injected embryos.
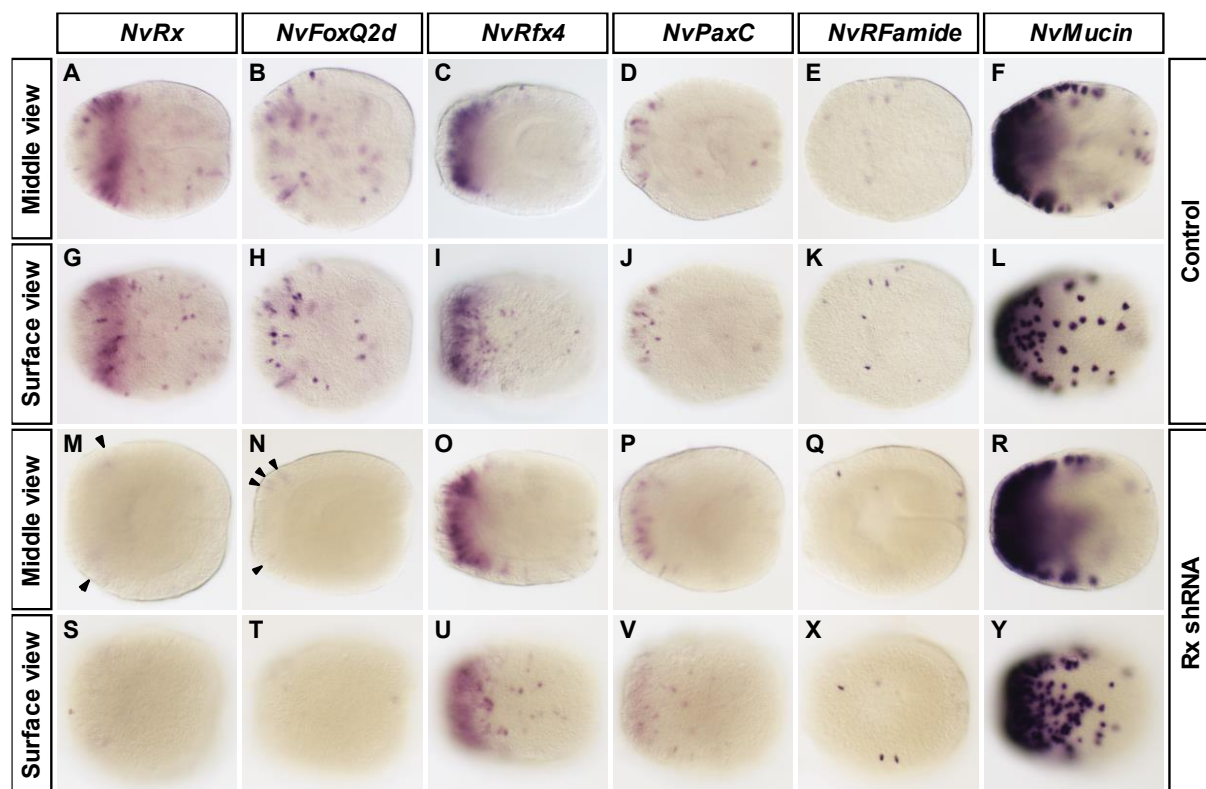

Figure 14: Colorimetric *in-situ* hybridization of early planula embryos injected with *NvRx* shRNA and *GFP* shRNA. Aboral pole is located on the left of the animal and the oral opening is located on the right of the animal. **A-L** shows the middle and surface view of sh*GFP* injected embryos. **M-Y** shows the middle and surface view of sh*NvRx* injected embryos. **(A-F):** *NvRx* expression in control samples **(A, G)**, is observed to have a band of expression on the aboral side of the embryo, with cells being observed throughout the ectoderm. *NvFoxQ2d* expression in control samples **(B, H)**, is observed as a handful of scattered cells throughout the embryo, with most cells being located on the aboral side. *NvRfx4* expression in control samples **(C, I)**, is observed as a dense cluster of cells in the aboral ectoderm of the embryo. Some cells can be observed on the oral side of the animal around the pharynx. *NvPaxC* expression in control samples **(D-J)**, can be observed as a cluster of cells in the aboral ectoderm of the embryo, with some cells found on the oral side of the animal. *NvRFamide* expression in control samples **(E-K)**, can be observed as a handful of scattered cells in the ectoderm. *NvMucin* expression in control samples **(F, L)**,

can be observed as a dense cluster of cells on the aboral ectoderm, with a few cells expressed in the pharynx. **(M-Y):** Injection of sh*NvRx* caused a visible reduction of *NvRx* expression **(M, S)** and *NvFoxQ2d* **(N, T)**. Injection of sh*NvRx* did not have an effect on *NvRfx4* **(O, U)**, *NvPaxC* **(P, V)**, *NvRFamide* **(Q, X)** and *NvMucin* **(R, Y)**.

4.3.1 Quantification

To quantify the effects on gene expression, the staining of individual embryos at gastrula stage was classified into three categories depending on the level of expression. Specimens where expression could not be observed were classified as "No expression". sh*NvRx* specimens that had roughly the same relative expression strength and/or the same number of cells as the average sh*GFP* injected sample were classified as "Full expression". sh*NvRx* injected specimens that fell in-between these categories were classified as "Reduced expression". Embryos observed with damage were not counted.

Looking at the *NvRx* stained specimens (**Figure 15**), (N_{shGFP}=85, N_{shNvRx}=144), one can observe that approximately 91% of sh*GFP* injected specimens exhibited full expression of *NvRx*, with approximately 9% showing no expression. Looking at sh*NvRx* injected specimens, approximately 69% showed no expression, approximately 24% of the samples showed reduced expression, and approximately 7% of the samples showed full expression. *NvRfx4,* (N_{shGFP}=77, N_{shNvRx}=91), and *NvPaxC,* (N_{shGFP}=68, N_{shNvRx}=124), stained embryos showed no significant difference in observed expression. Looking at *NvFoxQ2d* stained samples, (N_{shGFP}=81, N_{shNvRx}=148), approximately 46% of samples injected with sh*NvRx* exhibited no expression. Due to so few observable *NvFoxQ2d*-positive cells at 30hpf, determining reduced- vs full expression was futile using the light microscope. Samples showing any expression was therefore categorized as full expression.
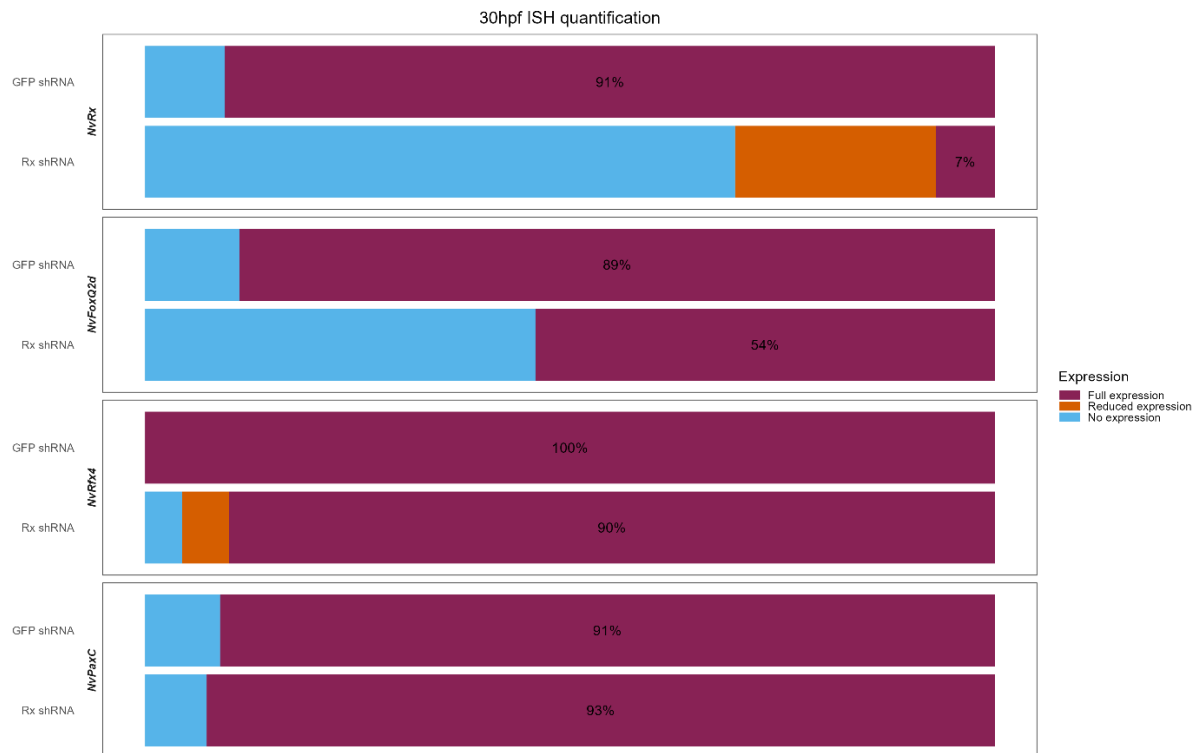
Figure 15: **Quantification of expression observed in 30hpf *in-situ* hybridization samples.** Samples were classified into three classes of expression. "Full expression" indicates same expression as control samples (*GFP* shRNA), "No expression" indicates no visible expression when observed through a light microscope, and "Reduced expression" indicates samples that fell in-between full- and no expression. *NvPaxC,* (N_{shGFP}=86, N_{shNvRx}=124), and *NvRfx4,* (N_{shGFP}=77, N_{shNvRx}=91), displayed no significant change in expression between sh*NvRx* and sh*GFP* injection, with ~90% of samples exhibiting full expression. *NvRx,* (N_{shGFP}=85, N_{shNvRx}=144), showed a drastic decrease in expression when injected with sh*NvRx* compared to sh*GFP*, with 31% of samples showing any expression. sh*NvRx* injection also led to a decrease in expression of *NvFoxQ2d* (N_{shGFP}=81, N_{shNvRx}=148), with 46% of samples showing no expression compared to 11% for sh*GFP* injected samples.

Looking at the 48hpf *NvRx* stained samples (**Figure 16**), (N_{shGFP}=79, N_{shNvRx}=78), one can observe a higher percentage of *NvRx* expression compared to the 30hpf samples. 20% of samples exhibited full expression and 40% had varying degrees of reduced expression. 40% of samples still were classified as having no expression under the stereo microscope, but when imaged at the compound microscope most of the samples showed some faint expression. Neither *NvRfx4,* (N_{shGFP}=65, N_{shNvRx}=63), *NvRFamide,* (N_{shGFP}=28, N_{shNvRx}=88), *NvMucin,* (N_{shGFP}=55, N_{shNvRx}=34), or *NvPaxC,* (N_{shGFP}=41, N_{shNvRx}=95), displayed any significant change in expression between sh*NvRx* and sh*GFP* injected samples. Compared to 30hpf *NvFoxQ2d* ISH samples, one can observe a higher percentage of samples exhibiting full expression in 48hpf *NvFoxQ2d,* (N_{shGFP}=64, N_{shNvRx}=69). 77% of samples had full expression, compared to 54% in 30hpf ISH, with 4% exhibiting reduced number of cells. When imaging, it was observed that almost all samples categorized under "No expression" had weak expression in cells that was not observed through the stereo microscope.
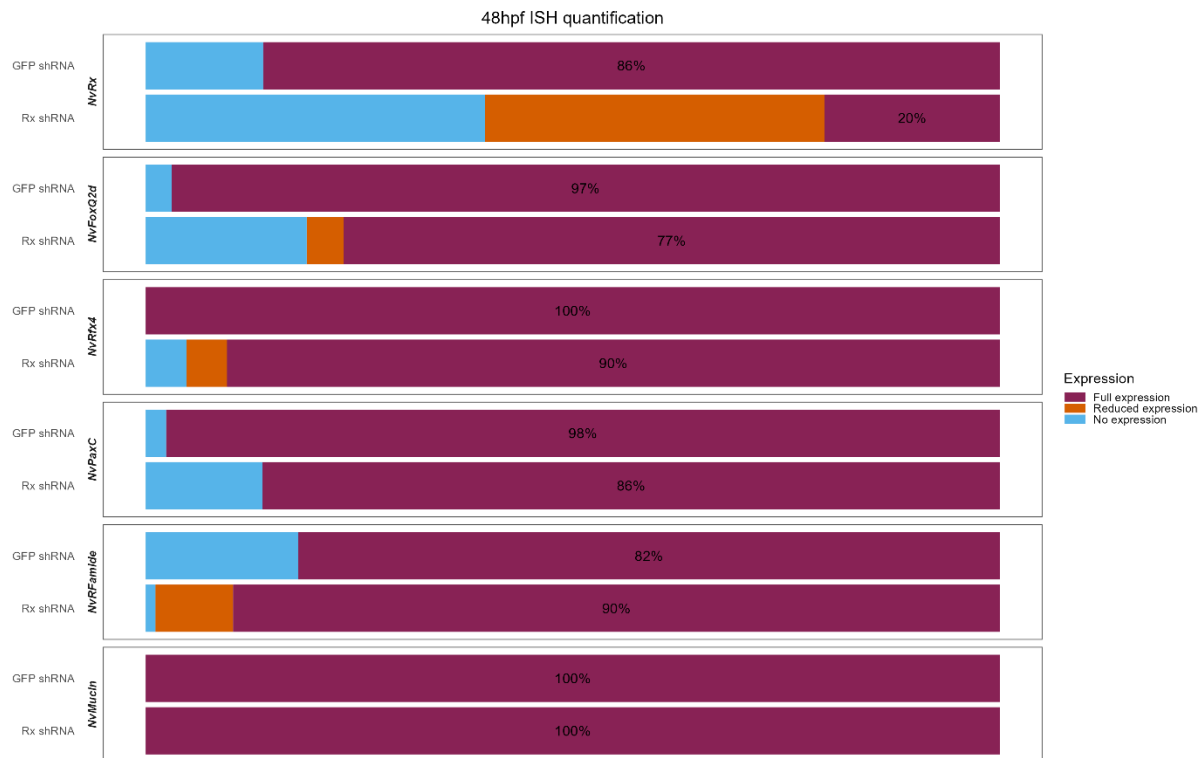
Figure 16: **Quantification of expression observed in 48hpf *in-situ* hybridization samples.** Samples were classified into three classes of expression. "Full expression" indicates same expression as control samples (GFP shRNA), "No expression" indicates no visible expression when observed through a stereo microscope, and "Reduced expression" indicates samples that fell in-between full- and no expression. *NvPaxC,* (N_{shGFP}=41, N_{shNvRx}=94), *NvRfx4,* (N_{shGFP}=65, N_{shNvRx}=63)*, NvRFamide,* (N_{shGFP}=28, N_{shNvRx}=88), and *NvMucin*, (N_{shGFP}=55, N_{shNvRx}=34), displayed no significant change in expression between sh*NvRx* and sh*GFP* injection, with ~90% of samples exhibiting full expression. *NvRx,* (N_{shGFP}=79, N_{shNvRx}=78), showed a decrease in expression when injected with sh*NvRx* compared to sh*GFP*, with 20% of samples showing full expression and 40% showing reduced expression. *NvFoxQ2d,* (N_{shGFP}=64, N_{shNvRx}=69), expression is also observed to be decreased, with 19% of samples showing no expression and 4% showing reduced expression compared to 13% of samples showing no expression when injected with sh*GFP*.

4.4 qPCR

A qPCR experiment was performed to give further quantitative information alongside the *in-situ* hybridization (**Figure 17**). Fertilized WT eggs were injected with sh*NvRx* and sh*GFP* and raised to 30hpf before RNA was extracted from the samples. Complimentary DNA (cDNA) was synthesised, and gene expression levels were compared between control samples with injected samples.

Looking at the *NvRx* values, one can see a mean log2 fold change value of negative 2.2. This indicates that the sh*NvRx* was successful in silencing the gene expression of *NvRx*. *NvRfx4* expression does not seem to be affected by the silencing, with a mean log2 fold change value negative 0.2. *NvPaxC* expression appears to be slightly downregulated, with a mean log2 fold change value of negative 0.9. Even though no change in expression was found during the ISH, this indicates some regulation of *NvPaxC* by *NvRx*. One puzzling result is the *NvFoxQ2d* expression. During the *in-situ* hybridization, the

expression of *NvFoxQ2d* was found to be downregulated by *NvRx* silencing. The result from the qPCR, a mean log2 fold change value of 0.6, contradicts the observations made during the *in-situ*.
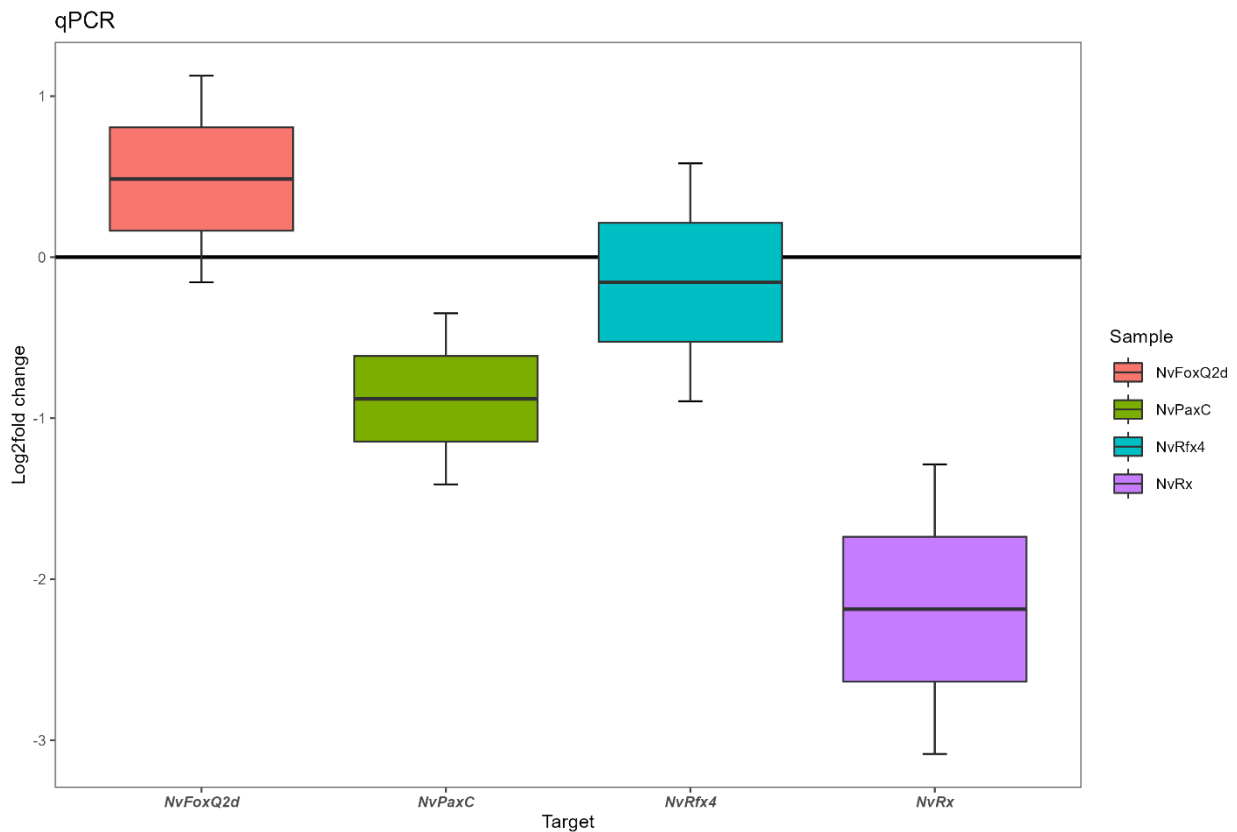

Figure 17: Boxplot showing log2 fold change values of genes in *NvRx* shRNA injected animals. *NvRx* was found to be downregulated, with a mean value of -2.2. A slight downregulation was found for *NvPaxC*, with a mean value of -0.9. No change in expression was found in *NvRfx4*, with a mean value of -0.2. *NvFoxQ2d* was found to be slightly upregulated, with a mean value of 0.5.

4.5 CRISPR mutants

To further investigate the function of *NvRx*, CRISPR/Cas9 mediated knockout lines were produced. Five different sgRNA's were selected using the web-tool CRISPOR and injected into fertilized WT eggs. Two of the selected sgRNAs targeted exon 1, and the other three sgRNAs targeted exon2. Injected F0 animals were raised to primary polyp stage before genomic DNA (gDNA) was extracted from eight randomly chosen individuals to be used to screen for mutations. The remaining F0s were raised to sexual maturity.
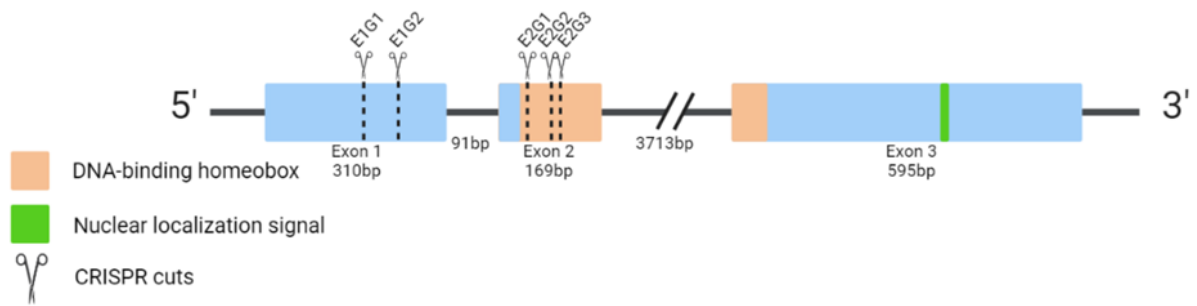
Figure 18: Illustration of *NvRx* and the sgRNA target locations. *NvRx* has a size of 4878bp, with three coding exons. Exons are shown as blue boxes, introns and UTRs are shown as lines. The DNA-binding homeobox is shown as orange boxes located on exon 2 and exon 3. Two sgRNA's (E1G1 and E1G2) were designed to target exon 1, and three sgRNA's (E2G1, E2G2 and E2G3) were designed to target exon two. Locations of CRISPR cuts are shown with scissors and dotted lines.

4.4.1 Melt curve analysis of CRISPR/Cas9 mutants.

A melt curve analysis was performed on the extracted gDNA to investigate the sgRNA injected lines for possible mutations. PCR was performed using primers flanking the expected mutation sites.

Six different F0 CRISPR lines were produced. For five of the lines, fertilized eggs were injected with a single sgRNA. By comparing the inflection point of injected samples against WT samples using melt curve analysis, one can observe if there has been a change to the genomic sequence. WT samples are expected to show one peak on the derivative melt curve plot, while mutated samples are expected to show multiple peaks, or a shifted melting point. All the lines exhibited signs of successful mutations of the gene sequence (**Figure 19**). 35 out of 40 injected samples tested were observed to be significantly different to the control samples.
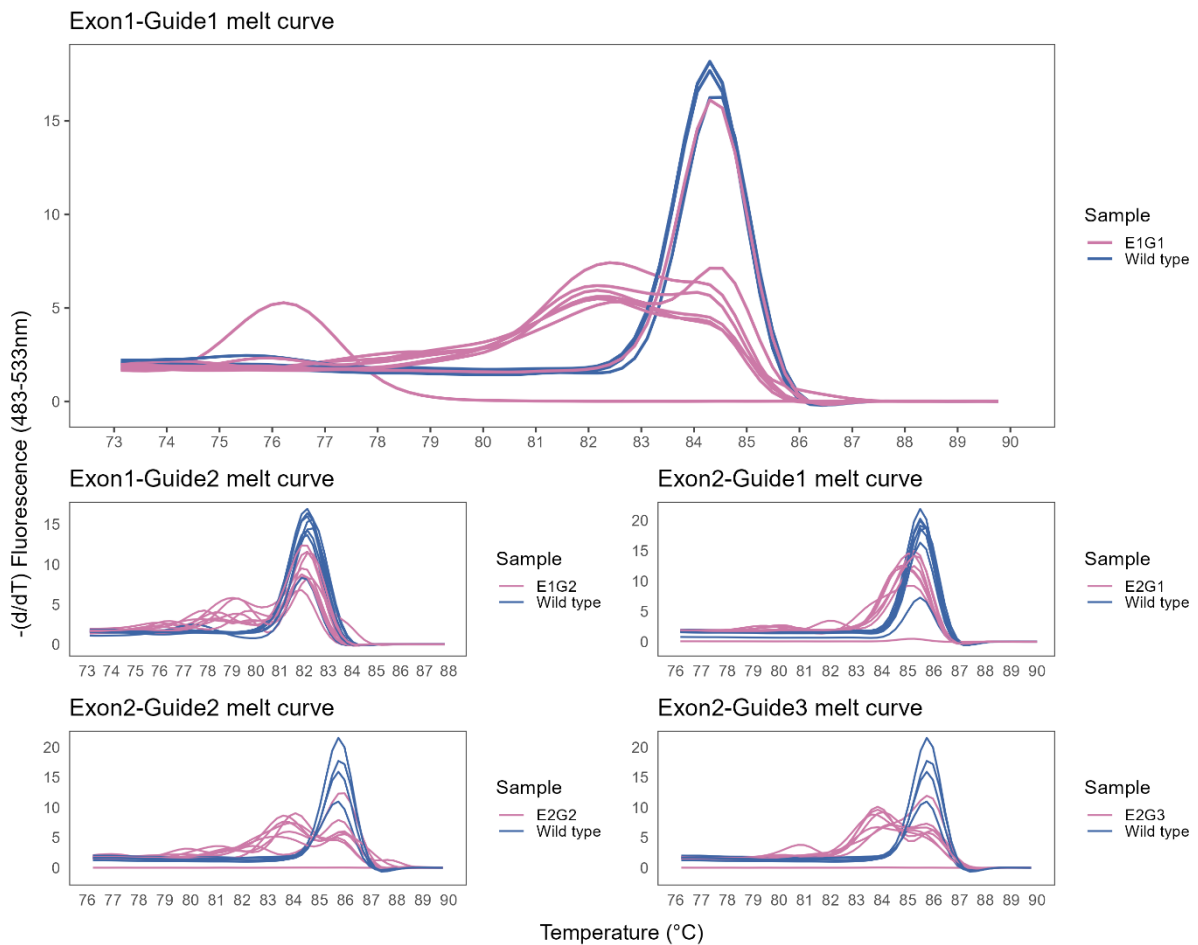
Figure 19: Melt curve analysis of samples subjected to CRISPR/Cas9 gene modification. Each melt curve in magenta is derived from the gDNA of an animal injected with the sgRNA indicated to the right, each blue melt curve is derived from a non-injected animal. Six out of eight samples tested in the Exon1-Gene1 (E1G1) line was observed to be positive for gene alterations. Eight out of eight samples tested from the E1G2 exhibited mutations. E2G1, E2G2 and E2G3 melt curves showed seven out of eight samples had mutations.

4.4.2 Generation of genomic deletion

Since the injection of a single sgRNA was successful, a double sgRNA injected line was proposed to delete parts of Exon1 and Exon 2. The injection of E1G1 and E2G3 would produce a roughly 350bp long deletion, ultimately causing a truncation of the protein, or the production of a protein that lacks most of the DNA-binding domain.

Because the change in the genetic sequence is so large, an agarose gel electrophoresis was performed. Looking at the gel (**Figure 20**), one can observe a band at approximately 1300bp on sample 2, 3, 5, and 8. This band corresponds to the WT gene sequence. In sample 2,3 and 8, one can observe a band at roughly 900bp. This matches the length of the mutated sequence. A band at roughly 700bp can be observed in sample 5. Sample 1, 4, 6 and 8 did not show any bands in the ranges expected. Four of the samples showed successful deletion.
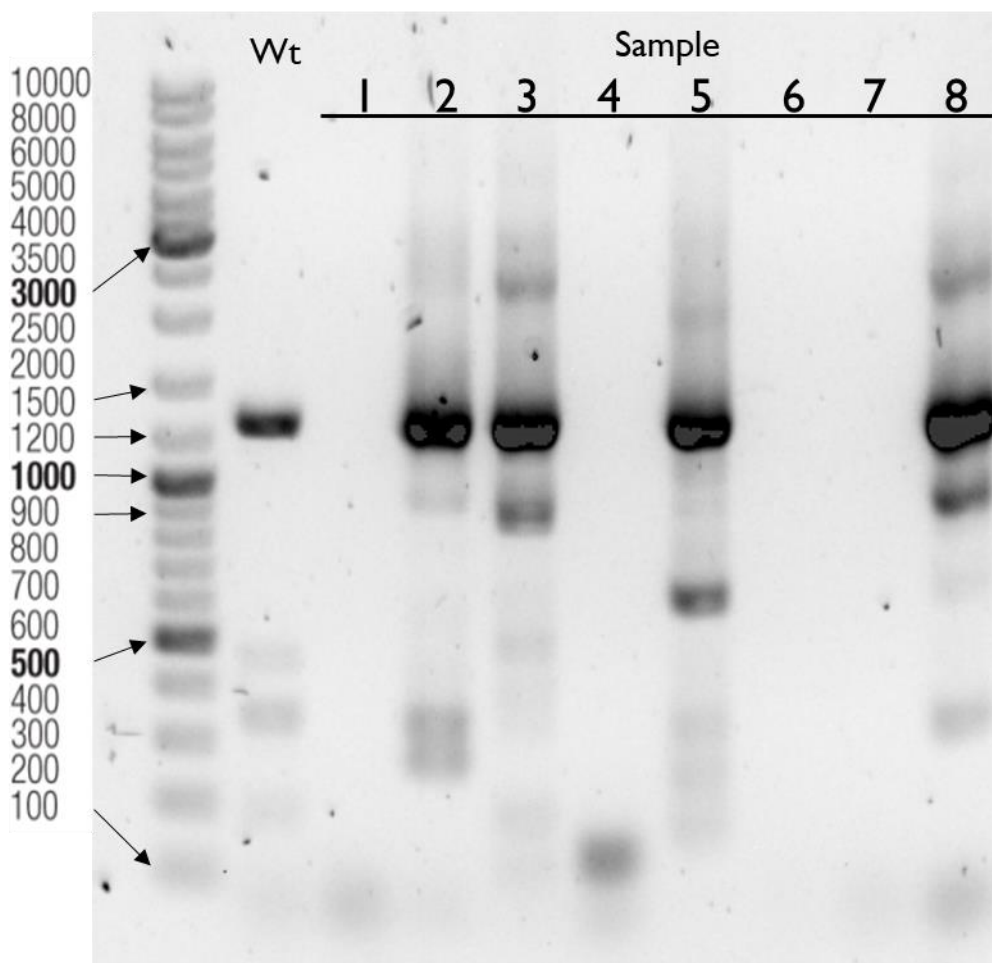
Figure 20: Agarose gel electrophoresis of double sgRNA/Cas9 injected animals. Eight samples injected with E1G1 and E2G3 sgRNA was tested for positive deletion. Bands at 1300bp corresponds to the WT gene sequence, while bands at 900 corresponds to the length of the mutated sequence. Samples 2,3, and 8 show evidence of successful deletion. Sample 5 shows a band at ~700 which is suspected to be a successful deletion. Samples 1,4,6 and 7 did not show any WT bands.

5 Discussion

Retinal homeobox plays an important role in the formation of the retina and retinal progenitor cells in vertebrates (Mathers et al., 1997). While multiple functional studies of Retinal homeobox have been performed in vertebrates, the function of *NvRx* in *Nematostella vectensis* has to our knowledge not been studied. As no specific structures for light detection have been observed in *Nematostella vectensis*, it points to *NvRx* playing a different role than vertebrate *Rx*. *NvRx* has been found to be highly upregulated in a sub-population of neurons expressing the neuronal marker *NvFoxQ2d* (Gahan, Kouzel, Bartsch and Rentzsch, unpublished data). In this study, we analysed the expression pattern of *NvRx* at an improved temporal resolution compared to earlier studies. We also showed that *NvFoxQ2d* partially co-localizes with *NvRx* expression, and that *NvRx* appears to act as an upstream regulator of *NvFoxQ2d*. Multiple lines of *NvRx* gene mutants were also successfully generated by CRISPR/Cas9-mediated genome editing.

5.1 *NvSoxB2* is expressed before the onset of *NvRx* expression

Mazza et al., were the first to identify and characterize the ortholog of vertebrate Retinal homeobox in *Nematostella vectensis*. In their colorimetric ISH, they found *NvRx* expression to start between early and mid-gastrula in *Nematostella vectensis* (Mazza et al., 2010). In their study, they did not indicate whether they looked at the stages between first cleavages and early gastrula stage (**Figure 5B,C**). We therefore wanted to replicate this experiment and determine the expression pattern at an improved temporal resolution. For our colorimetric ISH, we investigated the expression of *NvRx* at the timepoint "mid-blastula" (12hpf) to "late planula" (96hpf) (**Figure 6**). Expression was observed as a uniform band on the aboral side of the animal in the mid and late gastrula stages. In the planula stages, expression was observed as scattered cells located mostly on the aboral side of the animal. Expression was not observed in the blastula stages, indicating that expression of *NvRx* starts between early and mid-gastrula. These observations are consistent with the finding of Mazza et al.

We also performed a colorimetric ISH of the neural progenitor marker *NvSoxB2* at the same timepoints as *NvRx* to compare temporal and spatial expression between them (**Figure 6**). The expression pattern of *NvSoxB2* has been documented before, and our ISH results show the same expression pattern observed in these studies, although with weaker signal (Magie et al., 2005; Richards & Rentzsch, 2014). Comparing the temporal expression of *NvSoxB2* and *NvRx*, we can see that *NvSoxB2* expression starts at the early to mid-blastula stage, whereas *NvRx* expression starts at early to mid-gastrula stage. This suggests that *NvRx* is not expressed in the early neural progenitor cells, which is compatible with our hypothesis that *NvRx* functions at a later timepoint in the development of neural cells. In a previous

study comparing animals with increased and decreased neurogenesis, it was found that morpholino mediated knockdown of *NvSoxB2* caused a reduction of *NvRx* expression (Richards and Rentzsch, personal communication). These results suggests that *NvSoxB2* acts as an upstream regulator of *NvRx*, either directly or indirectly. To test this hypothesis, a double fluorescence ISH could be performed to look for co-expression, or shRNA mediated knockdown of *NvSoxB2* to confirm the morpholino experiment.

5.2 *NvRx* appears to be an upstream regulator of the transcription factor *NvFoxQ2d*

To investigate the hypothesis that *NvFoxQ2d* and *NvRx* are expressed in the same cells, double fluorescence ISH was performed on late gastrula-, early planula- and mid-planula stage WT embryos (**Figure 7-Figure 9**). The fluorescence ISH revealed that the majority of *NvFoxQ2d*-positive cells showed co-expression with *NvRx*, however this co-expression was not exclusively mutual. *NvRx* was found to be expressed in other cells not expressing *NvFoxQ2d*, especially in the late gastrula and mid-planula.

To further investigate the connection between *NvRx* and *NvFoxQ2d*, a knockdown experiment was performed using sh*NvRx* injections. If *NvRx* plays a role in regulating the expression of *NvFoxQ2d,* we would assume that the silencing of *NvRx* expression will have an effect on *NvFoxQ2d* expression. The expression of each sample was quantified and categorized to give an idea about the effect of the shRNA injection. From the quantification of the colorimetric ISH performed on the shRNA injected samples (**Figure 15-Figure 16**), we observed a complete silencing of *NvRx* expression in 69% of the samples at the late gastrula stage, with 24% of the categorized samples showing reduced expression and 7% showing full expression (**Figure 15**). At the early planula stage (**Figure 16**), only 40% of injected samples displayed complete silencing of *NvRx*, with 40% showing reduced expression and 20% showing full expression. The lack of complete gene silencing indicates a sub-optimal shRNA design or heterogeneity in the injections, something that can be improved in future studies either by designing a new shRNA, or by injecting multiple sh*RNA*s.

Nevertheless, when we compare the late gastrula *NvFoxQ2d* control samples against the sh*NvRx* injected samples, we can observe a complete silencing of *NvFoxQ2d* expression in 46% of the samples. At the early planula stage, the number of samples showing a complete silencing is reduced to 19%, with 4% of samples showing reduced expression. If *NvFoxQ2d* is in fact regulated by *NvRx*, this reduction in silenced samples could be attributed to the wear-off of the shRNA. Due to the few observable cells and the subjectiveness of the quantification step, it is also likely that some of the samples with reduced expression having been categorized with the "full expression" samples. In spite of that, these results suggest that *NvRx* functions as an upstream regulator of *NvFoxQ2d* either directly

or indirectly. The reason we don't see a stronger silencing of *NvFoxQ2d* can also be attributed to other TFs regulating *NvFoxQ2d* in a network with *NvRx*. To test this, double shRNA injections can be performed, and looking for a stronger downregulation.

To get a more objective quantification to support the ISH quantification, a qPCR was performed. Surprisingly, we found no significant downregulation of *NvFoxQ2d*. Two biological replications were performed with three technical replicates. Time constraints prevented us from performing the last triplicate, however, the average value of the log2 fold change was found to be 0.5 (**Figure 17**). For the moment, there is no satisfactory answer to this discrepancy observed between the ISH and qPCR. One thing that could be looked at in the future is the *NvFoxQ2d* primer efficiency. Additionally, a qPCR could be performed on the *NvRx* knockout mutants to look at the *NvFoxQ2d* expression.

As we can see from the expression pattern of *NvRx* in the gastrula stages (**Figure 6-Figure 13**), *NvRx* is expressed homogeneously in the lower part of the aboral half. This expression pattern is reminiscent of patterning genes, indicating that *NvRx* could play a role in patterning the aboral domain. If *NvRx* plays a role as a patterning gene, it would be reasonable to expect a disturbance in the aboral domain (i.e. the domain not being specified correctly) when *NvRx* is knocked down. This could lead to the absence of *NvFoxQ2d* expression observed in the *NvRx* knockdown. If this was the case, we would expect cells expressed in the aboral domain to be affected as well, however when we look at the *NvPaxC* expression, which partially overlaps with *NvRx* expression, we don't see a change in expression between the control and the *NvRx* knockdown. While this is not clear evidence against a patterning role for *NvRx,* it supports the hypothesis that *NvRx* plays a more specific role in the development of *NvFoxQ2d*-expressing cells. To further investigate if *NvRx* plays a patterning role, one could test other patterning genes, such as *NvSix3*/*6, NvFoxQ2a* and *NvFoxD1* among others, in *NvRx* knockdown specimens.

5.3 No evidence for a broader role of *NvRx* in the development of neural and secretory cells

In addition to looking at the connection between *NvRx* and *NvFoxQ2d*, we also investigated if *NvRx* acts as an upstream regulator of other transcription factors upregulated in the *NvFoxQ2d*-expressing cell population. As *NvRx* is observed to be expressed more broadly than in just the *NvFoxQ2d*-expressing population, we also wanted to investigate if *NvRx* plays a role in other cell types, such as neurons and secretory cells. For the late gastrula stage ISH, we looked at the expression of *NvRfx4* and *NvPaxC* after sh*NvRx* injection (**Figure 13**), while in early planula stage ISH we looked at the expression of *NvRfx4* and *NvPaxC,* alongside genes known to be expressed in neurons (*NvRFamide*), and in

secretory cells (*NvMucin*) (**Figure 14**). *NvRfx4* expression is observed as a dense cluster of cells in the aboral ectoderm in both late gastrula and early planula, with no significant difference observed between the control and sh*NvRx* injected animals for *NvRfx4*. Some variance in cell count can be observed in **Figure 13** and **Figure 14**, however this is thought to be natural expression variance and was observed within the sample-group as well. *NvPaxC* expression is observed as a small number of cells scattered in the ectoderm in the late gastrula, and as a cluster of cells mostly on the aboral pole in the early planula. No significant difference could be observed between the sh*NvRx* injected specimens and control specimens in the *in-situ* hybridization, however, the qPCR shows a small downregulation with a log2 fold change of -0.9. The number of *NvPaxC*-expressing cells in late gastrula have been observed to have high natural variability within the same sample-group, and this can explain this result.

Because *NvRx* has been observed in cells not expressing *NvFoxQ2d,* we decided to investigate *NvRFamide,* a neuropeptide marker, and *NvMucin* expressed in gland cells, in the early planula ISH. *NvRFamide* expression is observed as a handful of cells scattered across the ectoderm. No significant difference could be observed in either numbers of cells or in expression pattern. *NvMucin* expression is observed as a dense cluster of cells on the aboral half of the animal, with scattered cells in the oral half of the animal. No difference in expression could be observed between the sh*NvRx* injected samples and control samples. An attempt was made to look at the effect *NvRx* could have on *NvElav1* (data not shown), however, we observed a high variance between biological replicates and decided not to pursue further investigation using ISH. No evidence was found supporting a broader role of *NvRx* in these cell types, however, *NvRx* might not regulate these specific genes we looked at. There is also the possibility that the transcription factors we looked at are functioning upstream of *NvRx*.

5.4 *NvRx* and *NvElav1*-expressing cells are found in close proximity to each other

As we have observed *NvRx* expression in cells not positive for *NvFoxQ2d* expression, we wanted to examine the possibility of *NvRx* being expressed in other neural cells. Fluorescence *in-situ* hybridization was performed on late gastrula-, early planula- and mid-planula stage WT embryos (**Figure 10-Figure 12**). Here, we observe a large number of *NvElav1* and *NvRx*-expressing cells in close proximity to each other, with one cell expressing both *NvRx* and NvElav1 (**Figure 11**). One possibility that could lead to these observations, is that *NvElav1*-expressing cells and *NvRx*-expressing cells originate from the same progenitor cell. For future studies it would be interesting to test whether *NvRx* and *NvElav1* are descendants from the same pool of progenitor cells, or if these cells are just found close to each other naturally. To investigate this hypothesis further, the *NvElav1::mOrange* transgenic reporter line (Nakanishi et al., 2012) could be crossed to a *NvRx::GFP* transgenic reporter

line, which is being generated at this moment. Crossing those transgenic reporter lines, followed by an immunostaining, would enable a closer examination of *NvElav1* and *NvRx* than the fluorescence ISH performed in this study.

5.5 Mutant *NvRx*-animals were successfully created by CRISPR/Cas9

To further understand the function of *NvRx* in *Nematostella*, mutant lines were created using the CRISPR/Cas9 system. Five lines were generated by injection of different single sgRNAs targeting |the first exon and the start of the second exon, respectively. The sixth line was injected with two sgRNA's, in hopes of creating a 350bp deletion. A melt curve analysis was performed on the extracted gDNA to investigate the single-injected lines for possible mutations. 35 out of 40 injected samples tested were observed to be significantly different to the control samples, confirming that changes to the DNA sequence had occurred in all five single-injected lines (**Figure 19**). For the double-injected line, a PCR followed by gel-electrophoresis was performed due to the expected size of the deletion. 4 out of 8 samples tested was observed to have a significantly shorter gene sequence (**Figure 20**). The F0 animals were then raised to sexual maturity. Due to the generation time of *Nematostella* and the allotted time for this master thesis, this was where this experiment ended. The animals were handed over to the lab group, who will continue this experiment. The continued experiment would involve crossing the remaining F0s with WT animals. Tissue samples of F1s would then be sequenced, and animals positive for mutations would be in-crossed to obtain homozygous mutants. These homozygous F2s could then be used to further investigate the function of *NvRx*.

It would be interesting to use these mutants to test if there is a more severe phenotype in the knockouts compared to the knockdowns, or if there are other TFs working as a regulatory network alongside *NvRx* driving the expression of *NvFoxQ2d*. The *NvRx* knockdown mutants will also allow us to look at the effect of gene silencing at later stages of development.

5.6 Conclusion and future perspectives

In this study, we intended to obtain new insight into the function of the transcription factor Retinal homeobox in *Nematostella vectensis.* Our leading hypothesis was that *NvRx* could play a role in the development of the *NvFoxQ2d*-expressing cell population. Our results show that the majority of *NvFoxQ2d*-expressing cells co-expressed *NvRx*, and through a knockdown experiment using *NvRx* shRNA we show that *NvFoxQ2d* is downregulated, indicating that *NvRx* plays a role in activating the transcription factor *NvFoxQ2d* either directly or indirectly. We also found *NvRx* to be expressed in cells

in close proximity to *NvElav1*-expressing cells, indicating that these might come from the same pool of progenitor cells.

It would be interesting to see if *NvRx*-expressing cells, or a subset of them, are proliferating, as many *NvFoxQ2d*-expressing cells are proliferating. This could be tested by EdU labelling, which reveals nascent DNA. By EdU labelling in a *NvRx* transgenic reporter line, or in combination with ISH for *NvRx*, we could determine if these cells are in a pre-mitotic phase. A *NvRx::GFP* transgenic reporter line is in progress at the time of writing, which could be used for this experiment. This transgenic line could also be helpful in determining the expression pattern of NvRx in more detail, and the morphology of the *NvRx*-expressing cells.

Because Retinal homeobox is necessary in the development of vertebrate eye structures, it would be interesting to investigate if *NvRx* knockout mutants are able to detect light. Even though no specific structures for light detection have been observed in *Nematostella vectensis*, we know that they can sense light, as one of the triggers for gametogenesis is light exposure (Fritzenwanker & Technau, 2002). If *NvRx* is found to hinder Nematostella from sensing light, it could point to *Rx* being conserved in photo sensory structures.

In this thesis we mainly looked at the function *NvRx* plays in the *NvFoxQ2d*-expressing cells, however *NvRx* is expressed more broadly, and in the future it could be interesting to characterize other cell types expressing *NvRx.*

6 References

Amberger, J. S., Bocchini, C. A., Scott, A. F., & Hamosh, A. (2019). OMIM.org: leveraging knowledge across phenotype–gene relationships. *Nucleic Acids Research*, *47*(D1), D1038–D1043. https://doi.org/10.1093/NAR/GKY1151

Bailey, T. J., El-Hodiri, H., Zhang, L., Shah, R., Mathers, P. H., & Jamrich, M. (2004). Regulation of development by Rx genes. *International Journal of Developmental Biology*, *48*(8–9), 761–770. https://doi.org/10.1387/IJDB.041878TB

Busengdal, H., & Rentzsch, F. (2017). Unipotent progenitors contribute to the generation of sensory cell types in the nervous system of the cnidarian Nematostella vectensis. *Developmental Biology*, *431*(1), 59–68. https://doi.org/10.1016/j.ydbio.2017.08.021

Campbell, N. A., Urry, L. A., Cain, M. L., Wasserman, S. A., Minorsky, P. V, & Reece, J. B. (2018). *Biology : a global approach* (11. ed., G). Pearson Education.

Casarosa, S., Amato, M. A., Andreazzoli, M., Gestri, G., Barsacchi, G., & Cremisi, F. (2003). Xrx1 controls proliferation and multipotency of retinal progenitors. *Molecular and Cellular Neuroscience*, *22*(1), 25–36. https://doi.org/10.1016/S1044-7431(02)00025-8

Concordet, J. P., & Haeussler, M. (2018). CRISPOR: intuitive guide selection for CRISPR/Cas9 genome editing experiments and screens. *Nucleic Acids Research*, *46*(W1), W242–W245. https://doi.org/10.1093/NAR/GKY354

Danno, H., Michiue, T., Hitachi, K., Yukita, A., Ishiura, S., & Asashima, M. (2008). Molecular links among the causative genes for ocular malformation: Otx2 and Sox2 coregulate Rax expression. *Proceedings of the National Academy of Sciences of the United States of America*, *105*(14), 5408–5413. https://doi.org/10.1073/PNAS.0710954105/SUPPL_FILE/0710954105SI.PDF

Fredman, D., Schwaiger, M., Rentzsch, F., & Technau, U. (2013). *Nematostella vectensis transcriptome and gene models v2.0.* https://figshare.com/articles/dataset/Nematostella_vectensis_transcriptome_and_gene_models_v2_0/807696

Fritzenwanker, J. H., & Technau, U. (2002). Induction of gametogenesis in the basal cnidarian Nematostella vectensis(Anthozoa). *Development Genes and Evolution*, *212*(2), 99–103. https://doi.org/10.1007/S00427-002-0214-7

Furukawa, T., Kozak, C. A., & Cepko, C. L. (1997). rax, a novel paired-type homeobox gene, shows expression in the anterior neural fold and developing retina. *Proceedings of the National Academy of Sciences of the United States of America*, *94*(7), 3088–3093. https://doi.org/10.1073/PNAS.94.7.3088

Hand, C., & Uhlinger, K. R. (1992). The culture, sexual and asexual reproduction, and growth of the sea anemone Nematostella vectensis. *Biological Bulletin*, *182*(2), 169–176. https://doi.org/10.2307/1542110

Hartenstein, V., & Stollewerk, A. (2015). The Evolution of Early Neurogenesis. *Developmental Cell*, *32*(4), 390. https://doi.org/10.1016/J.DEVCEL.2015.02.004

Kelava, I., Rentzsch, F., & Technau, U. (2015). Evolution of eumetazoan nervous systems: insights from cnidarians. *Philosophical Transactions of the Royal Society B: Biological Sciences*, *370*(1684). https://doi.org/10.1098/RSTB.2015.0065

Kessler, C. (1994). Non-radioactive analysis of biomolecules. *Journal of Biotechnology*, *35*(2–3), 165–189. https://doi.org/10.1016/0168-1656(94)90034-5

Kristan, W. B. (2016). Early evolution of neurons. *Current Biology*, *26*(20), R949–R954. https://doi.org/10.1016/j.cub.2016.05.030

Layden, M. J., Boekhout, M., & Martindale, M. Q. (2012). Nematostella vectensis achaete-scute homolog NvashA regulates embryonic ectodermal neurogenesis and represents an ancient component of the metazoan neural specification pathway. *Development*, *139*(5), 1013–1022. https://doi.org/10.1242/DEV.073221

Layden, M. J., Rentzsch, F., & Röttinger, E. (2016). The rise of the starlet sea anemone Nematostella vectensis as a model system to investigate development and regeneration. *Wiley Interdisciplinary Reviews. Developmental Biology*, *5*(4), 408. https://doi.org/10.1002/WDEV.222

Lee, P. N., Kumburegama, S., Marlow, H. Q., Martindale, M. Q., & Wikramanayake, A. H. (2007). Asymmetric developmental potential along the animal–vegetal axis in the anthozoan cnidarian, Nematostella vectensis, is mediated by Dishevelled. *Developmental Biology*, *310*(1), 169–186. https://doi.org/10.1016/J.YDBIO.2007.05.040

Lodish, H., Bretscher, A., Ploegh, H., Amon, A., Martin, K. C., Kaiser, C. A., Krieger, M., & Berk, A. (2016). *Molecular cell biology* (8th ed.). W.H. Freeman & Co. Ltd.

Loosli, F., Winkler, S., Burgtorf, C., Wurmbach, E., Ansorge, W., Henrich, T., Grabher, C., Arendt, D., Carl, M., Krone, A., Grzebisz, E., & Wittbrodt, J. (2001). Medaka eyeless is the key factor linking retinal determination and eye growth. *Development*, *128*(20), 4035–4044. https://doi.org/10.1242/DEV.128.20.4035

Loosli, Felix, Staub, W., Finger-Baier, K. C., Ober, E. A., Verkade, H., Wittbrodt, J., & Baier, H. (2003). Loss of eyes in zebrafish caused by mutation of chokh/rx3. *EMBO Reports*, *4*(9), 894. https://doi.org/10.1038/SJ.EMBOR.EMBOR919

Magie, C. R., Pang, K., & Martindale, M. Q. (2005). Genomic inventory and expression of Sox and Fox genes in the cnidarian Nematostella vectensis. *Development Genes and Evolution*, *215*(12), 618–630. https://doi.org/10.1007/S00427-005-0022-Y/FIGURES/6

Martindale, M. Q., Pang, K., & Finnerty, J. R. (2004). Investigating the origins of triploblasty: `mesodermal' gene expression in a diploblastic animal, the sea anemone Nematostella vectensis(phylum, Cnidaria; class, Anthozoa). *Development*, *131*(10), 2463–2474. https://doi.org/10.1242/DEV.01119

Mathers, P. H., Grinberg, A., Mahon, K. A., & Jamrich, M. (1997). The Rx homeobox gene is essential for vertebrate eye development. *Nature 1997 387:6633*, *387*(6633), 603–607. https://doi.org/10.1038/42475

Matus, D. Q., Pang, K., Daly, M., & Martindale, M. Q. (2007). Expression of Pax gene family members in the anthozoan cnidarian, Nematostella vectensis. *Evolution & Development*, *9*(1), 25–38. https://doi.org/10.1111/j.1525-142X.2006.00135.x

Mazza, M. E., Pang, K., Reitzel, A. M., Martindale, M. Q., & Finnerty, J. R. (2010). A conserved cluster of three PRD-class homeobox genes (homeobrain, rx and orthopedia) in the Cnidaria and Protostomia. *EvoDevo*, *1*(1), 1–15. https://doi.org/10.1186/2041-9139-1-3

Nakanishi, N., Renfer, E., Technau, U., & Rentzsch, F. (2012). Nervous systems of the sea anemone Nematostella vectensis are generated by ectoderm and endoderm and shaped by distinct mechanisms. *Development*, *139*(2), 347–357. https://doi.org/10.1242/DEV.071902

Ohuchi, H., Tomonari, S., Itoh, H., Mikawa, T., & Noji, S. (1999). Identification of chick rax/rx genes with overlapping patterns of expression during early eye and brain development. *Mechanisms of Development*, *85*(1–2), 193–195. https://doi.org/10.1016/S0925-4773(99)00094-5

Paridaen, J. T., & Huttner, W. B. (2014). Neurogenesis during development of the vertebrate central nervous system. *EMBO Reports*, *15*(4), 351–364. https://doi.org/10.1002/EMBR.201438447

Rahimi-Balaei, M., Bergen, H., Kong, J., & Marzban, H. (2018). Neuronal migration during development of the cerebellum. *Frontiers in Cellular Neuroscience*, *12*, 484. https://doi.org/10.3389/FNCEL.2018.00484/BIBTEX

Redwine, J. M., & Evans, C. F. (2002). Markers of central nervous system glia and neurons in vivo during normal and pathological conditions. *Current Topics in Microbiology and Immunology*, *265*, 119–140. https://doi.org/10.1007/978-3-662-09525-6_6/COVER

Reitzel, A. M., Burton, P. M., Krone, C., & Finnerty, J. R. (2007). Comparison of developmental trajectories in the starlet sea anemone Nematostella vectensis: embryogenesis, regeneration, and two forms of asexual fission. *Invertebrate Biology*, *126*(2), 99–112. https://doi.org/10.1111/J.1744-7410.2007.00081.X

Rentzsch, F., Layden, M., & Manuel, M. (2017). The cellular and molecular basis of cnidarian neurogenesis. *Wiley Interdisciplinary Reviews: Developmental Biology*, *6*(1), 1–19. https://doi.org/10.1002/wdev.257

Rentzsch, F., Renfer, E., & Technau, U. (2020). Generating Transgenic Reporter Lines for Studying Nervous System Development in the Cnidarian Nematostella vectensis. *Methods in Molecular Biology (Clifton, N.J.)*, *2047*, 45–57. https://doi.org/10.1007/978-1-4939-9732-9_3

Richards, G. S., & Rentzsch, F. (2014). *Transgenic analysis of a SoxB gene reveals neural progenitor cells in the cnidarian Nematostella vectensis*. https://doi.org/10.1242/dev.112029

Richards, G. S., & Rentzsch, F. (2015). Regulation of Nematostella neural progenitors by SoxB, Notch and bHLH genes. *Development*, *142*(19), 3332–3342. https://doi.org/10.1242/DEV.123745

Röttinger, E. (2021). Nematostella vectensis, an Emerging Model for Deciphering the Molecular and Cellular Mechanisms Underlying Whole-Body Regeneration. *Cells*, *10*(10). https://doi.org/10.3390/CELLS10102692

Ryan, J. F., Burton, P. M., Mazza, M. E., Kwong, G. K., Mullikin, J. C., & Finnerty, J. R. (2006). The cnidarian-bilaterian ancestor possessed at least 56 homeoboxes: evidence from the starlet sea anemone, Nematostella vectensis. *Genome Biology*, *7*(7), R64. https://doi.org/10.1186/gb-2006-7-7-R64

Steinmetz, P. R. H., Aman, A., Kraus, J. E. M., & Technau, U. (2017). Gut-like ectodermal tissue in a sea anemone challenges germ layer homology. *Nature Ecology & Evolution*, *1*(10), 1535–1542. https://doi.org/10.1038/s41559-017-0285-5

Technau, U. (2020). Gastrulation and germ layer formation in the sea anemone Nematostella vectensis and other cnidarians. *Mechanisms of Development*, *163*, 103628. https://doi.org/10.1016/J.MOD.2020.103628

Technau, U., & Steele, R. E. (2011). Evolutionary crossroads in developmental biology: Cnidaria. *Development*, *138*(8), 1447–1458. https://doi.org/10.1242/dev.048959

Tournière, O., Gahan, J. M., Busengdal, H., Bartsch, N., & Rentzsch, F. (2022). Insm1-expressing neurons and secretory cells develop from a common pool of progenitors in the sea anemone Nematostella vectensis. *Science Advances*, *8*(16). https://doi.org/10.1126/sciadv.abi7109